Czech Technical University in Prague

Faculty of Nuclear Sciences and Physical Engineering

Department of Physics
Study Programme: Nuclear and Particle Physics

Studies of collectivity via azimuthal correlations of charged particles in small collision systems

Studium kolektivních jevů pomocí azimutálních korelací nabitých částic v malých srážkových systémech

DIPLOMA THESIS

Author: Bc. Daniel Mihatsch
Supervisor: Ing. Katarína Křížková Gajdošová, Ph.D.
Academic year: 2022/2023

ZADÁNÍ DIPLOMOVÉ PRÁCE

Student: Bc. Daniel Mihatsch

Studijní program: Jaderná a částicová fyzika

Název práce:
(česky)

Studium kolektivních jevů pomocí azimutálních korelací nabitých částic v malých srážkových systémech

Název práce:
(anglicky)

Studies of collectivity via azimuthal correlations of charged particles in small collision systems

Pokyny pro vypracování:

1) Anizotropní tok a kolektivní jevy v relativistických jádro-jaderných srážkách na moderních urychlovačích

2) Známky kolektivity v relativistických srážkách malých systémů na moderních urychlovačích

3) Studium metody multi-částicových kumulantů pro výpočet anizotropního toku v modelu PYTHIA, především způsobů potlačení pozadí

4) Studium vlivu jetů na metodu multi-částicových kumulantů pro výpočet anizotropního toku

5) Diskuze výsledků studia metody v simulacích a srovnání s experimentálními daty
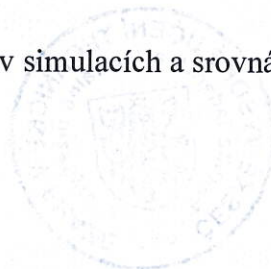
Doporučená literatura:

[1] S. Sarkar, H. Satz and B. Sinha: The Physics of the Quark-Gluon Plasma. Springer, 2010

[2] J. Nagle and W. Zajc: Small system collectivity in relativisticc hadronic and nuclear collisions. Annu. Rev. Nucl. Part. Sci. 68:1-36 (2018)

[3] T. Sjöstrand, et al.: An introduction to PYTHIA 8.2. Comput. Phys. Commun. 191, 159 (2015)

[4] A. Bilandzic, et. al.: Generic Framework for anisotropic flow analyses with multiparticle azimuthal correlations. Phys. Rev. C 89, 064904 (2014)

[5] J. Jia, et al.: Revealing long-range multiparticle collectivity in small collision systems via subevent cumulants. Phys. Rev. C 96, 034906 (2017)

Jméno a pracoviště vedoucího diplomové práce:

Ing. Katarína Křížková Gajdošová, Ph.D., Katedra fyziky
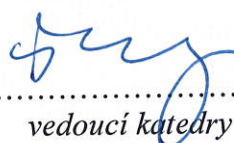Fakulta jaderná a fyzikálně inženýrská ČVUT v Praze

Datum zadání diplomové práce: 20.10.2021
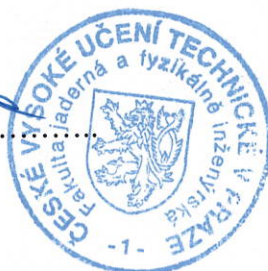
Termín odevzdání diplomové práce: 02.05.2022

Doba platnosti zadání je dva roky od data zadání.

....
garant studijního programu

....
vedoucí katedry

....
děkan

V Praze dne   20.10.2021

P R O H L Á Š E N Í

Já, níže podepsaný

Jméno a příjmení studenta: Daniel Mihatsch

Osobní číslo: 473991

Název studijního programu (oboru):   Jaderná a částicová fyzika

prohlašuji, že jsem diplomovou práci s názvem:

Studium kolektivních jevů pomocí azimutálních korelací nabitých částic v malých srážkových systémech

vypracoval samostatně a uvedl veškeré použité informační zdroje v souladu s Metodickým pokynem o dodržování etických principů při přípravě vysokoškolských závěrečných prací.

V Praze dne 2. 5. 2023   ....

                                              podpis

Acknowledgment

Název práce:

Studium kolektivních jevů pomocí azimutálních korelací nabitých částic v malých srážkových systémech

Autor: Bc. Daniel Mihatsch

Studijní program: Jaderná a částicová fyzika

Druh práce: Diplomová práce

Vedoucí práce: Ing. Katarína Křížková Gajdošová, Ph.D.
                Katedra fyziky, Fakulta jaderná a fyzikálně inženýrská, České vysoké učení technické v Praze

Abstrakt: Kolektivní jevy ve srážkách malých systémů byly rozsáhle studovány několika experimenty za účelem zkoumání možné přítomnosti silně interagujícího média podobného tomu, které vzniká při jádro-jaderných srážkách. Jednou z nejvhodnějších technik měření jsou multi-částicové kumulanty s využitím metody podudálostí pro potlačení non-flow kontaminace. Míra tohoto potlačení může záviset na akceptanci detektoru a zvolené konfiguraci podudálostí. V této práci prezentujeme výsledky naší studie těchto efektů na měření anizotropního toku s využitím multi-částicových kumulantů a metody podudálostí v závislosti na multiplicitě pp srážek generovaných v modelu PYTHIA. Navíc se zabýváme vlivem jetů, které tvoří největší část non-flow, s využitím knihovny FastJet. Naše zjištění pomohou v interpretaci experimentálních výsledků z různých experimentů and jejich vzájemnému srovnání, které je klíčové v současné debatě o původu kolektivity v malých srážkových systémech.

Klíčová slova: Malé srážkové systémy, anizotropní tok, metoda multi-částicových kumulantů, metoda podudálostí.

Title:

Studies of collectivity via azimuthal correlations of charged particles in small collision systems

Author: Bc. Daniel Mihatsch

Study Programme: Nuclear and Particle Physics

Sort of project: Diploma thesis

Supervisor: Ing. Katarína Křížková Gajdošová, Ph.D.
Department of Physics, Faculty of Nuclear Sciences and Physical Engineering, Czech Technical University in Prague

Abstract: Collective behaviour in collisions of small systems has been studied extensively by several experiments to address the possible existence of a strongly-interacting medium similar to that created in heavy-ion collisions. One of the most suitable measurement techniques are the multiparticle cumulants with the subevent method to suppress non-flow contamination. The amount of non-flow suppression may depend on the detector acceptance and the chosen subevent configuration. In this work, we will present our studies of such effects on flow measurements using multiparticle cumulants with the subevent method as a function of multiplicity in pp collisions generated with the PYTHIA model. In addition, the influence of jets, which are considered as the largest contributors to non-flow, will be investigated using the FastJet library. Our findings will help in interpretation of experimental results from different experiments and in their mutual comparison, which is crucial in the current debate about the origins of collectivity in small collision systems.

Key words: Small collision systems, anisotropic flow, method of multiparticle cumulants, subevent method.

Contents

Introduction

The collective behaviour observed in relativistic collisions of nuclei is expected to be linked to the presence of the Quark-Gluon Plasma (QGP), a state of matter in which quarks and gluons are not bounded in hadrons. The concept of collective flow and its origin are well described in heavy-ion collisions. Studies of collectivity also led to the invention of a very efficient and precise method of flow computation called the multiparticle cumulant method that uses azimuthal correlations between particles.

The turnaround happened in 2010, when the CMS collaboration observed signs of collectivity in proton-proton collisions, where the QGP was not expected to be created. Unlike the large systems that are relatively well explored, the origin of collectivity in small systems was not clear. It has started a new era of the investigation of small systems. The measurements of collective flow in small systems are heavily contaminated by short-range non-global correlations called non-flow. The non-flow background is mostly made up of correlations of decay products and correlations of particles that are constituents of jets. The multiparticle cumulant method, which reduces non-flow contamination by taking more particles into the correlation, has been shown to be insufficient to suppress such a strong non-flow background. A lot of effort has been put into finding a better way to suppress that background, leading to the most advanced method yet called the subevent method, which can be used together with the multiparticle cumulant method.

This work focuses on the investigation of the collective behaviour in collisions of small systems and more specifically on the suppression effect of the subevent method used along with the multiparticle cumulant method. Our aim is to investigate how different acceptances of detectors affect flow measurements and how robust is the subevent method to non-flow contamination. Finally, we are interested in the suppression effect of the subevent method on non-flow originating from correlations of particles in jets.

The first chapter is devoted to a brief introduction to relativistic hadron collisions, chapter 2 describes the concept of the collective flow and presents some recent recent results of flow collectivity measurements performed in heavy-ion collisions and small collision systems, chapter 3 introduces the method of multiparticle cumulants and the subevent method, chapter 4 is devoted to PYTHIA and FastJet tools, which are used in this work, chapter 5 presents our results of the investigation of influence of detector acceptance on a measurement and robustness of the subevent method and the last chapter is devoted to the study of suppression effect of the subevent method on jet related non-flow.

Chapter 1

Relativistic hadron collisions

Collisions of hadrons and nuclei at very high speed are being investigated for more than 50 years and nowadays thanks to many steps done in acceleration technology, enormous collision energies are achieved. These collisions are usually divided into two categories - heavy-ion collisions and small systems.

Heavy ions are nuclei consisting of a large number of nucleons, e.g. Gold, Uranium or Lead. In heavy-ion collisions are these nuclei accelerated almost to the speed of light and collided in accelerators. Large density of nucleons consisting of quarks and gluons and enormous amount of deposited kinetic energy leads to creation of extremely dense and hot medium, which is called quark-gluon plasma (QGP). In this state of matter, quarks and gluons are no longer bounded in hadrons and can move freely until the moment of freeze-out is reached.

Collisions of small systems are another case. In these pp or $p + A$ (A is an arbitrary nucleus) collisions, the system size and particle density are significantly smaller. Consequently, the evolution of these systems is faster, making it impossible to form the QGP in these collisions.

First part of introductory chapter is dedicated to the explanation of basic concepts of heavy-ion collisions such as evolution of the system, the creation of the QGP and phase diagram of nuclear matter. Second part is focused on collisions of small systems, especially on the development of motivation for the study of this type of collisions and important differences from heavy-ion collisions.

1.1 Heavy-ion collisions

1.1.1 Evolution of collision

All nuclei are composed of quarks and gluons, which are the elementary particles of the Standard Model. Gluons are mediators of the strong interaction carrying color charge - new quantum number introduced in quantum chromodynamics (QCD), which is a theory of the strong interaction. Very specific properties of the strong

interaction, resulting from the dependence of the coupling constant on energy, are a color confinement and an asymptotic freedom. Color confinement is the reason, why free quarks are not observed under usual conditions. If we want to move two quarks apart, we have to exert such a large force, and therefore deposit an energy that is sufficient for creation of a new quark-antiquark pair. Asymptotic freedom describes behavior in the opposite situation, when quarks are extremely close to each other. Since the coupling of the strong interaction is weaker the closer particles are, the enormous density of quarks can lead to the disengagement of quarks from hadrons and the formation of the QGP.

Let us now briefly describe the evolution of heavy-ion collision. Two beams of ultra-relativistic nuclei composed of a large number of nucleons are collided in a particle accelerator. A critical density of particles in the interaction point leads to the decoupling of quarks and subsequently to the formation of the QGP. Afterwards this medium begins to expand into the surrounding vacuum and consequently the temperature of the medium starts to decrease. Upon reaching $T \approx 151\,\mathrm{MeV}$ [1] a phase transition occurs, which means that quarks are engaged to hadrons. For a short period hadrons can interact inelastically with each other until the chemical freeze-out is reached. In the last period of the evolution hadrons interact elastically reaching the kinetic freeze-out at $T \approx 100\,\mathrm{MeV}$ [2]. Finally, all particles leave the interaction area and are detected in the detectors. The whole evolution is illustrated in the Fig. 1.1.
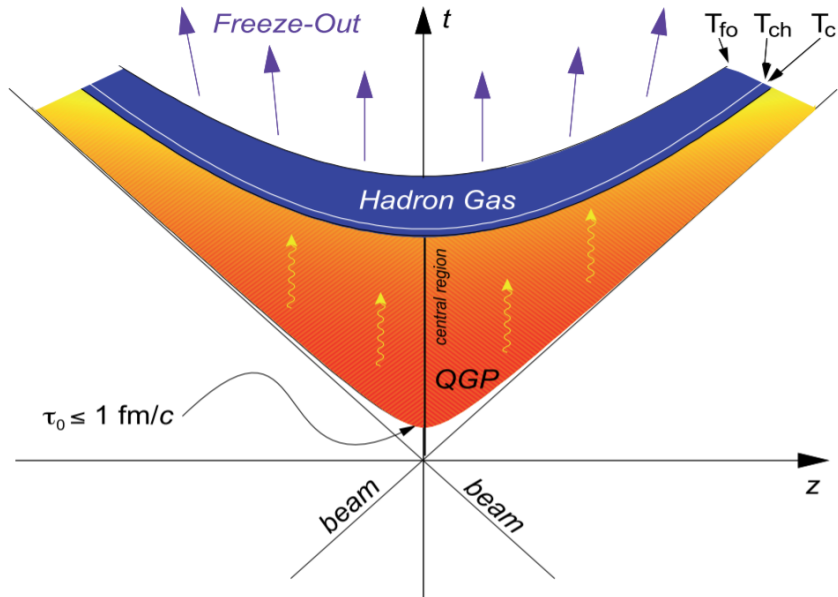
Figure 1.1: The evolution of heavy-ion collision [3].

1.1.2 Phase diagram of nuclear matter

The behavior of nuclear matter under different conditions is described in phase diagram in Fig. 1.2 in more detail. These conditions can be characterized by a

specific temperature and a baryo-chemical potential μ_B, which describes the balance between matter and antimatter in the system. At low energies of collided particles, almost all scattered particles can be identified with the initial ones, which means that the collision is nearly elastic. The opposite case are collisions of particles at high energies, where significant amount of particles is newly created in 1 to 1 ratio of matter and antimatter. In summary, low-energy collisions lead to the dominance of matter and therefore the value of baryo-chemical potential μ_B is high and high-energy collisions lead to the balance between matter and antimatter and therefore $\mu_B \approx 0$. For our purposes we can focus only on Hadron Gas area and Quark-Gluon Plasma area of the diagram and the line between those areas, which illustrates the phase transition. The phase transition line is divided into two parts by the critical point, which is supposed to be located between $\mu_B = 200\,\mathrm{MeV}$ and $\mu_B = 500\,\mathrm{MeV}$ [4]. In high-energy collisions, where the value of μ_B is smaller than the value associated with the critical point, the phase transition between parton-hadron region is rapid cross-over. In collisions, where μ_B is higher than the value associated with the critical point, the phase transition is of the first order.

The determination of exact position of the critical point is the subject of many current researches, e.g. RHIC Beam Energy Scan [5].
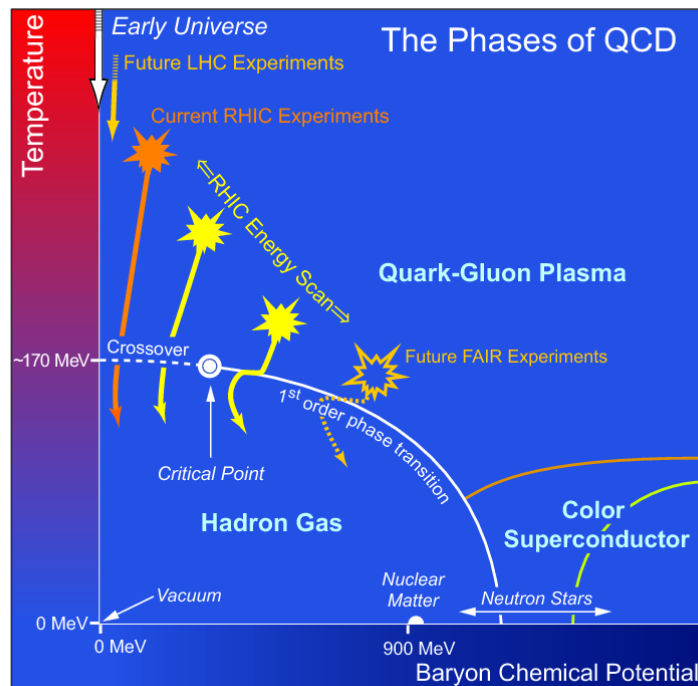
Figure 1.2: Phase diagram of nuclear matter [6].

1.2 Small collision systems

Collisions of protons and deuterons are being studied for many reasons including understanding the nature of the strong force by studying the jet substructure [7] or investigating the internal structure of nucleons [8]. But if we would like to focus only on the existence of the QGP and hydrodynamic approach used for the description of this state of matter, it is natural to expect big differences between heavy-ion collisions and small systems. The reasons for this expectation are as follows. Collisions of small systems such as pp, $p+A$ and $d+A$ contain a significantly smaller number of particles, which means that the sufficient particle and energy density for the creation of the QGP should not be achieved. Secondly, the lifetime of the medium possibly created in these collisions is very short and therefore termalization of the medium is highly unlikely to be achieved [9]. In summary, the only reasons to study collisions of small systems in the context of the QGP are measurements used for determination of parton distribution functions [10] or measurements of nuclear modification factor R_{AA}, which is usually defined as the ratio of the yield in heavy-ion collisions to the corresponding yield in pp collisions scaled by the number of binary nucleon-nucleon collisions [11].

The turnaround occurred in 2010, when the CMS collaboration examined two-particle correlations in high-multiplicity pp collisions [12]. The results showed that despite all expectations there is a hint of similarity between heavy-ion collisions and collisions of small systems. The signs of collective behavior associated with the hydrodynamic description of the QGP was now observed also in small systems. The unexpected discovery started a new era of the investigation of small systems. Measurements, that have been already done in heavy-ion collisions, are now studied in small systems exposing little by little the origin of collective behavior in all different small collision systems.

Chapter 2

Anisotropic flow

The whole evolution of heavy-ion collision described in previous chapter is extremely short process, e.g. duration of the QGP phase is of the order $\approx 10^{-24}$ s. So if we want to study what is happening in the interaction point right after the collision we cannot use standard methods of experimental nuclear physics such as scattering off external particles in the created medium. The only way to probe the QGP is to analyze the final-state particles with their properties. It helps us to understand what happened in each section of the evolution.

There are several ways how to probe the QGP using the list of detected particles, which can be in general divided into two categories - hard and soft probes. Hard probes include among others heavy flavour production or reconstructions of jets - collimated sprays of hadrons created as a result of fragmentation of an energetic parton. Soft probes include for example investigation of particle spectra, di-lepton production, or collective flow.

The last mentioned item, i.e. collective flow is the main subject of this diploma thesis. First part of the following chapter formulates what collective flow is and the second part is dedicated to comprehensive review of flow measurements both in heavy-ion collisions and collisions of small systems using data recorded at the LHC and RHIC.

2.1 Collective flow

The concept of collective flow is well described in heavy-ion collisions. After colliding two heavy nuclei, extremely dense and hot medium often referred to as a fireball is created at the point of interaction. Any collision can be characterized by impact parameter b, which is defined as the distance between the centers of nuclei. Since a significant part of collisions is peripheral ($0 < b < 2R$, where R denotes the radius of nuclei), elliptic spatial anisotropy is dominant for most collisions. At the same time, the distribution of nucleons in the collided nuclei fluctuates, which introduces additional spatial anisotropy of higher orders. Elliptic and triangular anisotropies, which are the most common ones, are illustrated in the left part of Fig. 2.1. Due to the

irregular shape of the fireball and the uneven distribution of nucleons, different pressure gradients arise in different directions. The medium is expanding anisotropically into the vacuum, i.e. at different velocities in different directions, transforming the spatial anisotropy of the initial-state into the final-state momentum and azimuthal anisotropy of emitted particles. Consequently, global correlations of azimuthal angles of particles can be observed and the resulting collective behavior is known as collective flow.
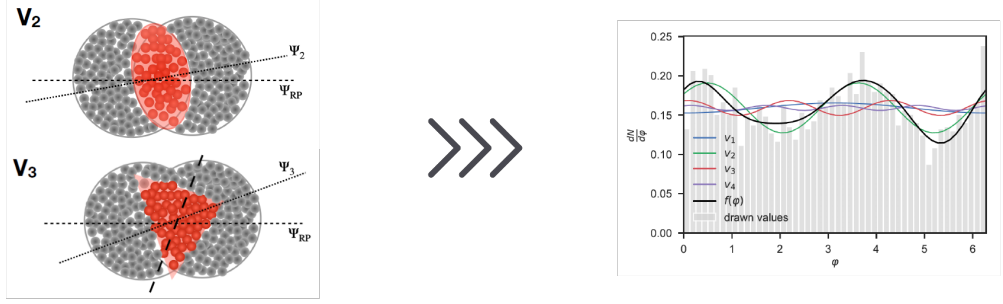
Figure 2.1: The creation of collective flow in heavy-ion collisions.

The azimuthal distribution of emitted particles can be further expanded into Fourier expansion (illustrated in the right part of Fig. 2.1)

$$\frac{\mathrm{d}N}{\mathrm{d}\varphi} \propto 1 + \sum_{n=1}^{\infty} 2v_n \cos\left[n(\varphi - \Psi_n)\right], \tag{2.1}$$

where φ is the azimuthal angle of produced particle in the transverse plane according to beam direction and Ψ_n is the orientation (angle) of the n-th symmetry plane corresponding to the Fourier coefficient v_n. Anisotropy of particle distribution is then characterized by Fourier coefficients v_n

$$v_n = \langle \cos\left[n(\varphi - \Psi_n)\right]\rangle, \tag{2.2}$$

where $\langle \cdot \rangle$ denotes average over all particles in particular collision. The most important flow coefficient for purposes of this diploma thesis is v_2, which is called elliptic flow from initial elliptic shape of overlap area of collided nuclei.

2.2 Review of recent collectivity measurements

2.2.1 Collective behaviour in heavy-ion collisions

Two-particle correlation

The first type of measurement of collective behavior in heavy-ion collisions worth mentioning is two-particle correlation as a function of difference of pseudorapidity $\Delta\eta$ and difference of azimuthal angle $\Delta\varphi$ between particles. The importance of this measurement will be clear after the section about collectivity in small collision systems, because it was this measurement that led to the discovery of collective behavior in small systems. Fig. 2.2 shows results of two-particle correlation for *Pb-Pb* collisions of pairs having $1 < p_T < 3$ GeV in $30-40\%$ centrality class. The significant peak around $(\Delta\eta, \Delta\varphi) \sim (0,0)$ arises from decays of high-p_T particles and jets. These correlations with low $\Delta\eta$ and $\Delta\varphi$ are called short-range correlations. Since collective flow is mostly associated with global long-range correlations (high $\Delta\eta$ and $\Delta\varphi$), this type of correlation is background in our measurements and will be further referred to as non-flow. The away-side jet peak, which should be located around $(\Delta\eta, \Delta\varphi) \sim (0, \pi)$, is smeared, so it is not easily visible. Other non-flow correlations such as decays of low-p_T particles contribute to these jet related correlations at $\Delta\varphi \sim \pi$. Behind all these non-flow correlations there is a characteristic two-ridge structure, where the first ridge denoted as away-side ridge is located at $\Delta\varphi \sim \pi$ and the second ridge denoted as near-side ridge is located at $\Delta\varphi \sim 0$. Both ridges reach up to high values of $\Delta\eta$ (indicated by the arrow). This structure is what we are looking for, because it is believed to arise from flow correlations and therefore it is the first important sign of collectivity in heavy-ion collisions. In fact, the two-ridge structure is a cosine modulation, which can be described by a Fourier expansion, from which the elliptic flow v_2 can be obtained. The two-ridge shape is also in an agreement with the idea of increased flow of particles along the minor-axis of the elliptical overlap area indicated in the introductory section [13].
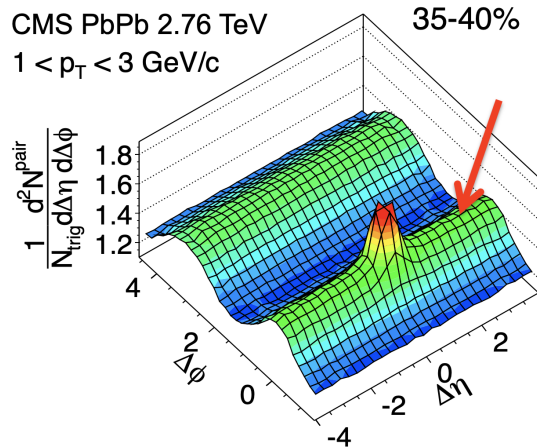

Figure 2.2: The measurement of two-particle correlation as a function of pseudorapidity difference $\Delta\eta$ and azimuthal angle difference $\Delta\varphi$ in *Pb-Pb* collisions [13].

Measurement of flow coefficients v_n

The second type of measurement is a measurement of flow coefficients v_n. The example is in Fig. 2.3, where measured dependence of v_2, v_3 and v_4 on centrality in *Pb-Pb* collisions at $\sqrt{s_{NN}} = 2.76\,\text{TeV}$ and $\sqrt{s_{NN}} = 5.02\,\text{TeV}$ are shown. The coefficient of elliptic flow $v_2\{2\}$ is computed from two-particle correlation using the multiparticle cumulant method, which will be described in chapter 3. $v_2\{4\}$, $v_2\{6\}$ and $v_2\{8\}$ are the same coefficients computed from four-particle, six-particle and eight-particle correlations, respectively. The non-flow short-range correlation in measurements using two-particle cumulant are suppressed by an η-separation $|\Delta\eta| > 1$ between particles.

Firstly, in Fig. 2.3 we can observe approximate equality of v_2, v_3 and v_4 in central collisions. It is associated with the fact that the anisotropy arises exclusively from the fluctuations of nucleon positions and there is no significant elliptic spatial anisotropy. The more peripheral the collision is, the more significant role the elliptic flow v_2 plays as the elliptic shape of overlap area is becoming more dominant. The results of v_2 computed from two-particle cumulants are generally lower than those obtained from multiparticle cumulants, especially in peripheral collisions. Since non-flow background is suppressed by the subevent method, the difference is related to the fluctuations of elliptic flow giving positive and negative contribution to two-particle and multiparticle cumulant, respectively [14].

The most important contribution of measurement of flow coefficients is determination of viscosity of the QGP. The viscosity divided by entropy η/s is obtained as a parameter of a theoretical hydrodynamical model fitted to measured data. Fig. 2.3 indicates good agreement between data and the model with temperature-dependent viscosity. However, the precise determination of the QGP viscosity is a great challenge because the theoretical models are dependent on many parameters, which should be determined in future detailed studies.

Elliptic flow of identified particles

The measurement of flow coefficients can be extended by studying p_T-dependence for different particle species separately. The example is in the Fig. 2.4, where we can observe p_T-dependence of elliptic flow in *Pb-Pb* collisions at $\sqrt{s_{NN}} = 5.02\,\text{TeV}$. We observe two phenomena attributed to the collective behaviour expected in heavy-ion collisions. The first one is mass ordering of low-p_T particles ($0.5 < p_T < 2.5\,\text{GeV/c}$). The lightest particles such as pions exhibit the highest elliptic flow and on the other hand the heaviest particles such as protons or lambda baryons exhibit the lowest elliptic flow. In a result we observe a solid dependency of low-p_T particles - the lighter the particle is, the easier it flows. The second phenomenon is observed for the particles in mid-p_T region and is called baryon-meson splitting. Between 2.5 and 5.0 GeV/c baryons exhibit generally higher v_2 values than mesons, which is associated with the different composition of these particle classes. In the extremely hot and dense QGP quarks are moving freely. Consequently, thanks to the expansion every quark should gain the same flow. This leads to the fact, that baryons composed of three quarks should carry more flow than mesons composed of two quarks only.
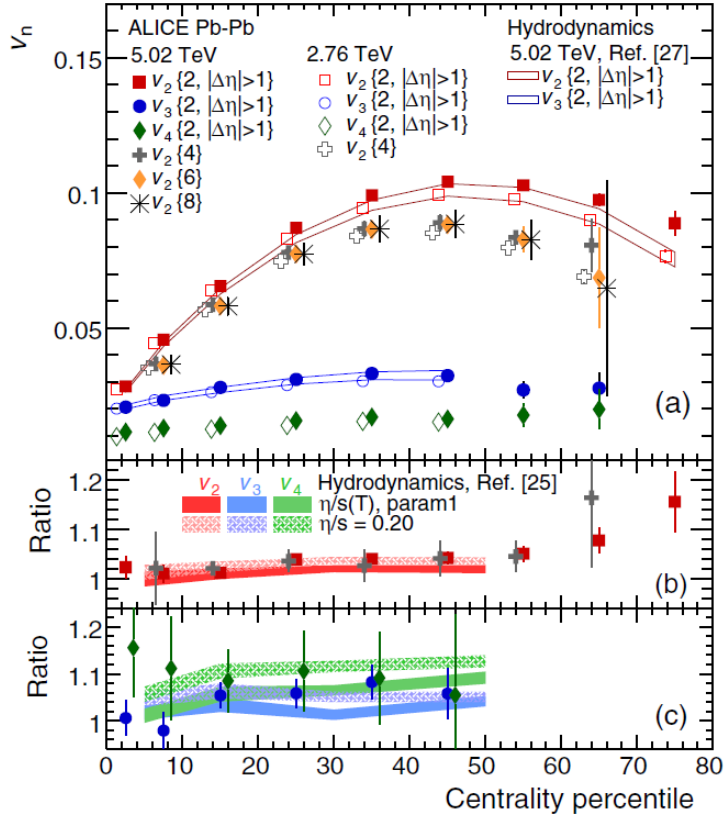
Figure 2.3: The measurement of flow coefficents v_n dependence on centrality in *Pb-Pb* collisions at $\sqrt{s_{NN}} = 2.76\,\text{GeV}$ and $\sqrt{s_{NN}} = 5.02\,\text{GeV}$ [14].

Measurement of 4-particle cumulant

Another example is a more detailed measurement of the 4-particle cumulant that can be calculated from the 4-particle correlation. Several measurements proved, that in heavy-ion collisions, where the QGP is expected to be created, the value of 4-particle cumulant is always negative (see section 3.2.2). Since 4-particle cumulant is by definition quite robust to non-flow and models without collectivity predict non-negative values of cumulant without any exception, we expect an essential link between negative value of 4-particle cumulant and existence of the QGP in heavy-ion collisions. The example of this measurement is showed in the Fig. 2.5, where the results of $c_2\{4\}$ dependence on multiplicity in *Pb-Pb* collisions at $\sqrt{s_{NN}} = 2.76\,\text{TeV}$ can be observed. The cumulant remains negative in all multiplicity classes except low-multiplicity events, where $N_{ch} < 60$. The system created in low-multiplicity collisions is too small to achieve the state of the QGP and therefore the collectivity is not observed.

Symmetric cumulants

The measurement of correlation between different orders of flow coefficients has proven to constrain parameters of hydrodynamical models [16], e.g. initial condi-
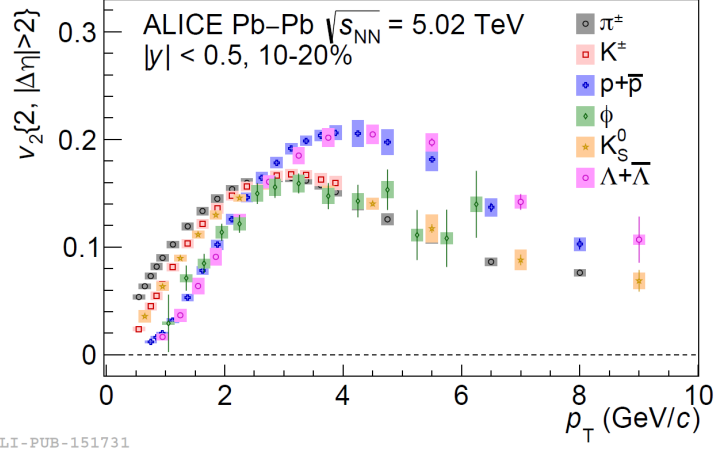
ALI-PUB-151731

Figure 2.4: The measurement of the elliptic flow v_2 of identified particles dependence on transverse momentum p_T in *Pb-Pb* collisions.
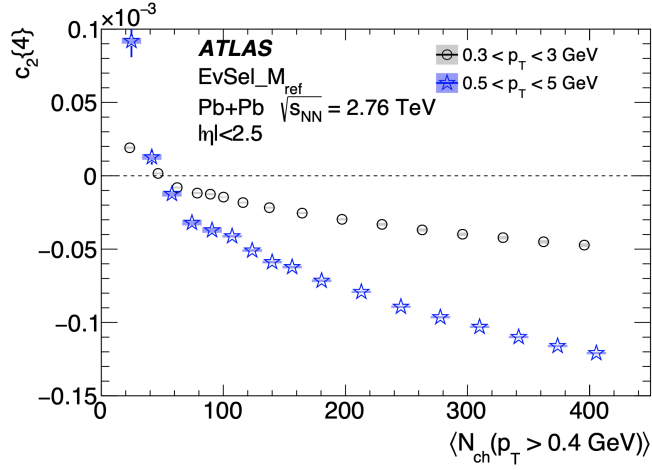
Figure 2.5: The measurement of 4-particle cumulant $c_2 4$ dependence on multiplicity in *Pb-Pb* collisions [15].

tions. The dependence of the correlation between v_2 and v_4 with or without the subevent method in *Pb-Pb* collisions at $\sqrt{s_{NN}} = 2.76$ TeV is shown in the Fig. 2.6 (left). The values of $SC_{2,4}\{4\}$ are mostly positive for all methods and the trend is increasing with $\langle N_{ch} \rangle$, which reflects previously shown increase of elliptic flow with multiplicity in heavy-ion collisions. The values obtained with the subevent method are lower, which is linked to the non-flow suppression. The right panel of the Fig. 2.6 shows the correlation between v_2 and v_3. The overall trend is decreasing with $\langle N_{ch} \rangle$ and results obtained using different methods are consistent. Uncertainties from non-flow are most significant in low-multiplicity region [17].
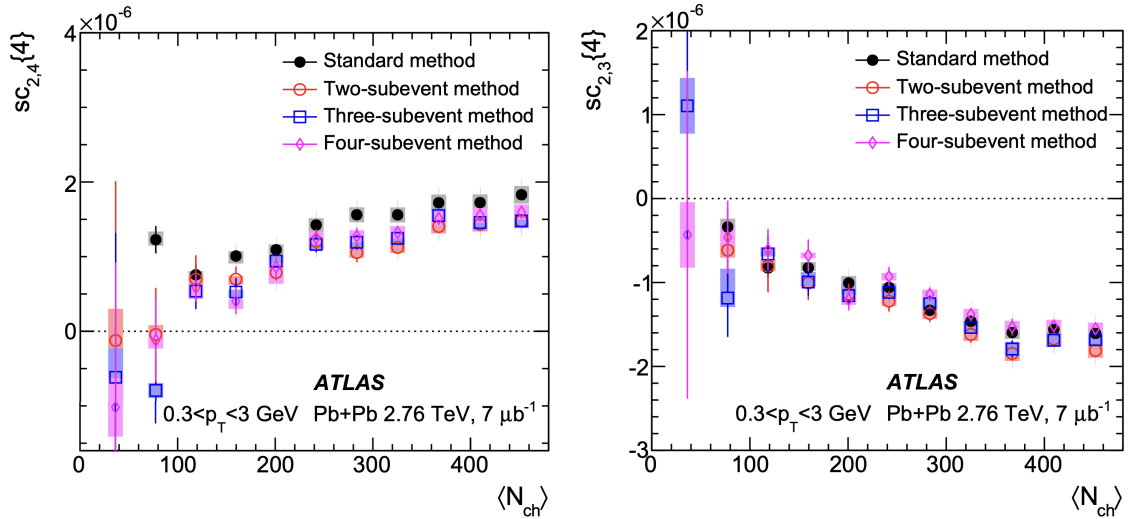
Figure 2.6: The measurement of $SC_{2,4}\{4\}$ (left) and $SC_{2,3}\{4\}$ (right) in *Pb-Pb* collisions at $\sqrt{s_{NN}} = 2.76\,\text{TeV}$ [17].

2.2.2 Collectivity in small collision systems

Two-particle correlation

The measurement of the two-particle correlation in high-multiplicity $p+p$ collisions in 2010 at CMS motivated the search for collective behaviour in small collision systems. Let us now illustrate this observation with more recent results of two-particle correlation in *pp* collisions from CMS in the Fig. 2.7. The left panel of the figure belongs to low multiplicity events, where we can observe significant peak near $(\Delta\eta, \Delta\varphi) \sim (0,0)$ resulting from jet fragmentation and decays of high-p_T particles similarly as in heavy-ion collisions. The away-side ridge representing decays of low-p_T particles and contributions from back-to-back jets can be also seen this measurement. But the significant difference between heavy-ion collisions and collisions of small systems is presence of near-side ridge. There is no hint of this ridge in low multiplicity measurement. But if we look at the results from high multiplicity events (the right panel of Fig. 2.7), we can observe, except for the previously mentioned, a hint of a long-range ridge structure of a low magnitude at $\Delta\varphi \sim 0$. This was the first hint of similarity of heavy-ion and small systems collisions [18].

The next logical step is to measure these correlations in different small systems such as proton-nuclei collisions. The results of *p-Pb* collisions from ALICE, ATLAS and CMS experiments are shown in the Fig. 2.8. The familiar structures such as jet peak at $(\Delta\eta, \Delta\varphi) \sim (0,0)$ and away-side ridge at $\Delta\varphi \sim \pi$ can be observed, but the most importantly the near-side ridge is present in these measurements too and its magnitude is about four time larger than in $p+p$ collisions. The fact of observation a near-side ridge in all results from three different experiments gives us compelling reason to further study, whether the collisions of small systems exhibits a similar collective behaviour to heavy-ion collisions [13].
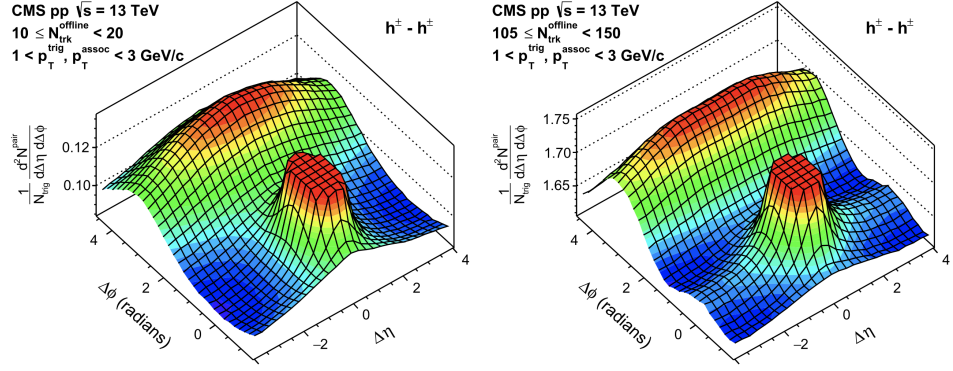
Figure 2.7: The measurement of two-particle correlation in *pp* low multiplicity (left) and high multiplicity (right) collisions [18].
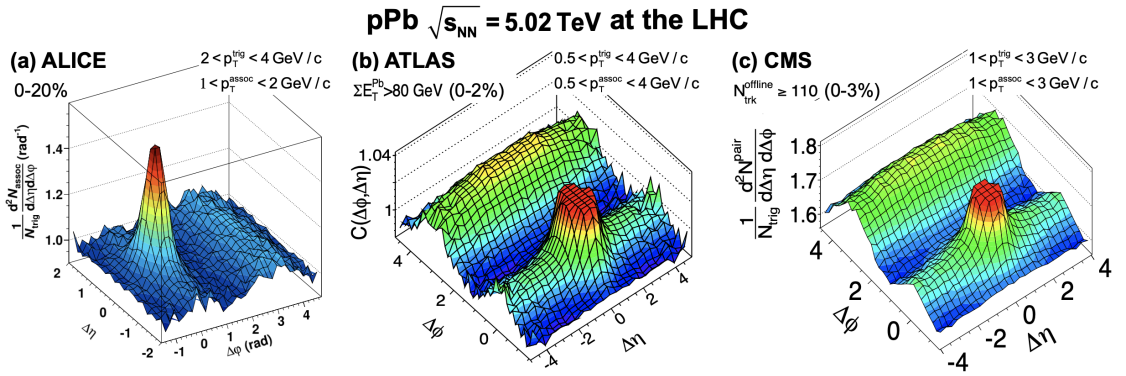
Figure 2.8: The two-particle correlation functions in high multiplicity *p-Pb* collisions measured by the ALICE (left) [19], ATLAS (middle) [20] and CMS (right) [21] experiments.

Measurement of flow coefficients v_n

The measurement of flow coefficients $v_2\{2\}$ (a), $v_3\{2\}$ (b), $v_4\{2\}$ (c) obtained from 2-particle cumulants and elliptic flow $v_2\{k\}$ from 4, 6 and 8-particle cumulants in *pp*, *p-Pb*, *Xe-Xe* and *Pb-Pb* collisions is shown in the Fig. 2.9, so we can easily compare the results for heavy-ion collisions and collisions of small systems.

Measurements corresponding to heavy-ion collisions (a-c) shows earlier mentioned multiplicity dependence of flow coefficient linked to the shape of the initial overlap region of the colliding nuclei. The dependence is most significant for elliptic flow, because the elliptical shape of the overlap is dominant. Another phenomenon observed in heavy-ion collisions is a magnitude ordering $v_2 > v_3 > v_4$. Results from small collision systems exhibit only a weak dependence of flow coefficients on multiplicity since the fluctuations of parton distribution in protons are independent of multiplicity. The magnitude ordering remains valid also in small systems. The comparison of experimental data from *pp* collisions with model calculation using PYTHIA 8 reveals a significant disagreement. This observation is consistent with the assumption that the measured signal is not only non-flow background.

The measurement of elliptic flow $v_2\{k\}$ in the Fig. 2.9 (d) is less influenced by non-flow effects, because it is computed from multiparticle cumulants. The results are consistent regardless of the number of particles taken into correlations and using or not using the subevent method in heavy-ion collisions. Thanks to the 3-subevent method a real-valued $v_2\{4\}$ can be computed even in low multiplicity p-Pb collisions, where the standard method provided a positive 4-particle cumulant. The consistence of the results of $v_2\{4\}$ and $v_2\{6\}$ in small systems indicates effective suppression of non-flow giving us another hint for collective behaviour in these collision systems [22], since in collective collisions there should be no dependence of v_2 on the number of particles in correlation.
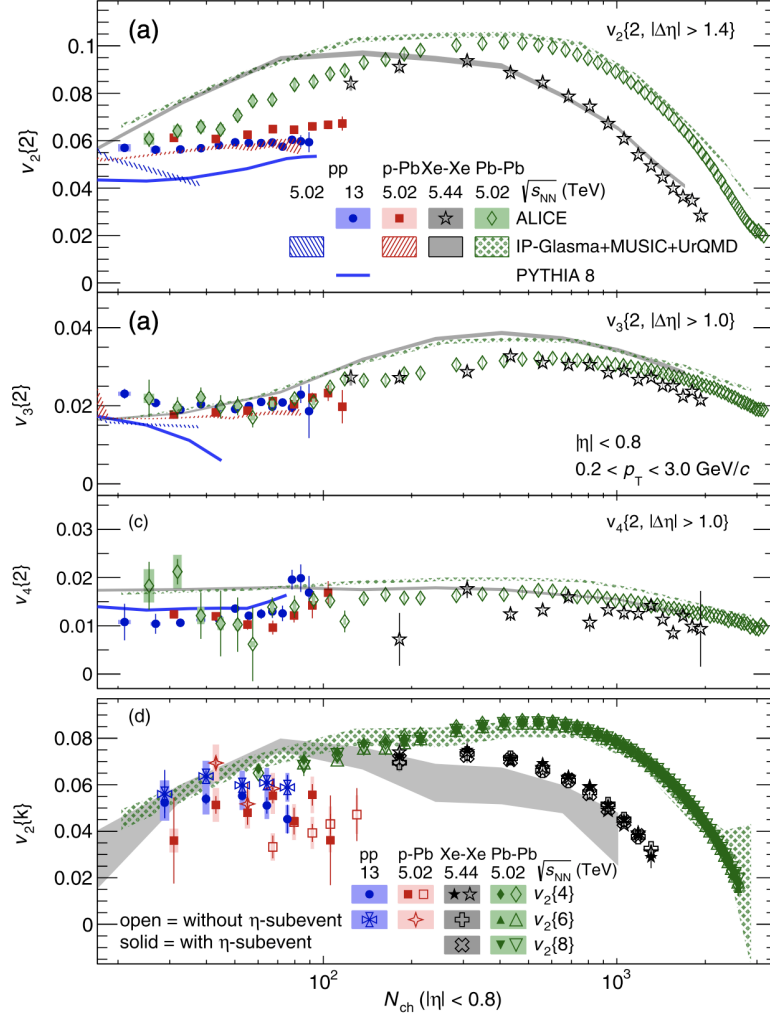
Figure 2.9: The flow coefficients $v_n\{k\}$ dependence on multiplicity in pp, p-Pb, Xe-Xe and Pb-Pb collisions [22].

Measurements of flow coefficients are studied also at PHENIX and STAR experiments. The Fig. 2.10 shows the dependence of v_2 and v_3 on transverse momentum p_T in high multiplicity p-Au, d-Au and He-Au collisions. The results provide a hint of transformation of the initial geometry into flow coefficients, e.g. the triangular shape of He nucleus in He-Au collisions takes effect in large magnitude of triangular flow in comparison to other measurements. The elliptical shape of deuteron

in *d-Au* collisions takes effect in large magnitude of elliptic flow. Finally, the round shape of proton in *p-Au* collisions leads to intermediate magnitude of both elliptic and triangular flow. The fact that the initial shape is strongly linked to the magnitude of coefficients indicates possibility to describe these systems in terms of hydrodynamics similarly as in heavy-ion collisions. In addition, the hydrodynamical models predict v_2 and v_3 measured at PHENIX quite well [23]. On the other hand, if we look at the data recently measured by the STAR experiment, we can observe that the measurement of v_3 is independent on the system size, which is linked to subnucleon fluctuations. In conclusion, these measurements could provide a hint of hydrodynamical evolution of the system, but we need much more investigation to understand it properly.
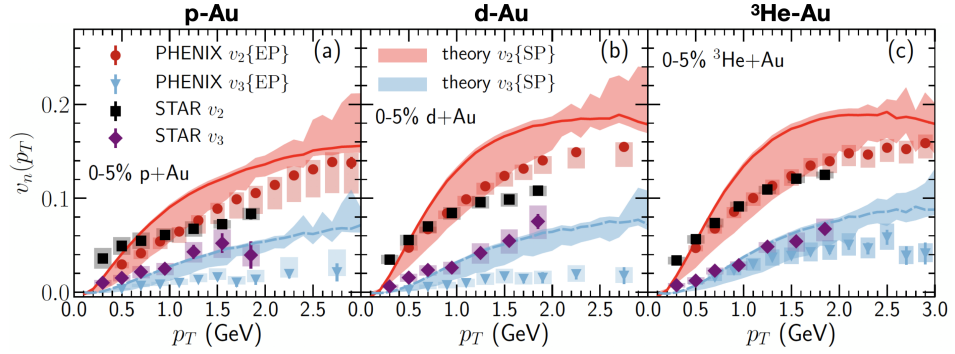
Figure 2.10: The elliptic and triangular flow dependence on transverse momentum p_T in high-multiplicity *p-Au*, *d-Au* and *He-Au* collisions [24].

Elliptic flow of identified particles

The differential elliptic flow of identified particles was recently measured at ALICE in collisions of small systems using ultra long-range di-hadron correlations to reduce the non-flow contamination. The phenomenon of mass ordering at low-p_T region can be observed in both *pp* (left) and *p-Pb* (right) collision in the Fig. 2.11. Similarly, at intermediate p_T region the baryon-meson splitting is clearly visible [25]. These observations provide another hint of collective behaviour in small systems.

Measurement of 4-particle cumulant

The negative value of 4-particle cumulant $c_2\{4\}$ is a significant sign of collective behaviour and always accompanies the presence of the QGP, but it is also a basic requirement to obtain a real value of elliptic flow as we will see in section 3.2.2. The first experiment that measured the negative value of $c_2\{4\}$ in collisions of small systems was the CMS experiment [18]. Other experiments at the LHC did not obtain similar results until the introduction of the 3-subevent method, which questioned the CMS results.
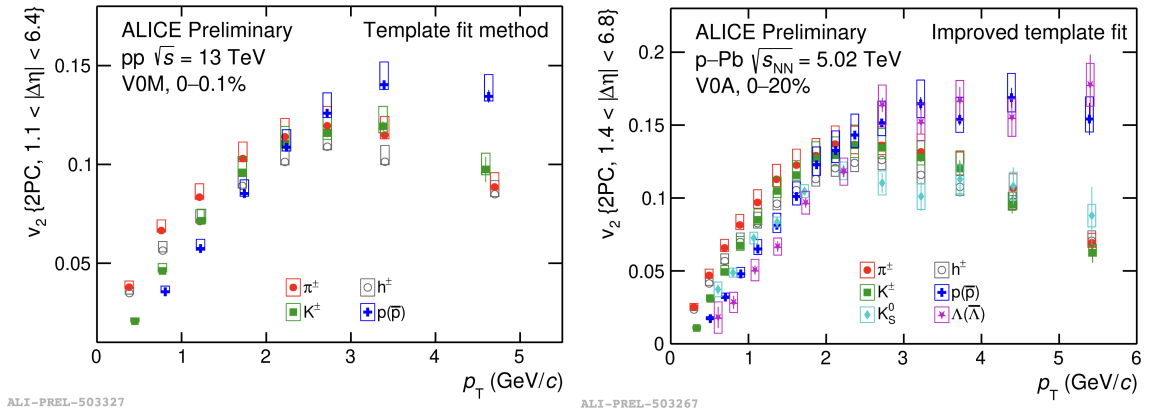
Figure 2.11: The elliptic flow of identified particles in high multiplicity *pp* (left) and *p-Pb* collisions [25].

In the Fig. 2.12 (left) is the dependence of 4-particle cumulant $c_2\{4\}$ on multiplicity in *pp* collisions for standard and subevent method measured by the ATLAS experiment. The values obtained using standard method are positive for all multiplicity classes. But the subevent method suppresses the positive contributions from non-flow background and consequently, the negative values of 4-particle cumulant are obtained for almost all multiplicity classes excluding low multiplicity events, which is consistent with the CMS results.

The similar measurement was done in *p-Pb* collisions and the results in the Fig. 2.12 (right) shows that the negative value of 4-particle cumulant is obtained in high multiplicity events even with the standard method. The 3-subevent method then effectively suppresses non-flow, which leads to negative 4-particle cumulant also in low multiplicity events.
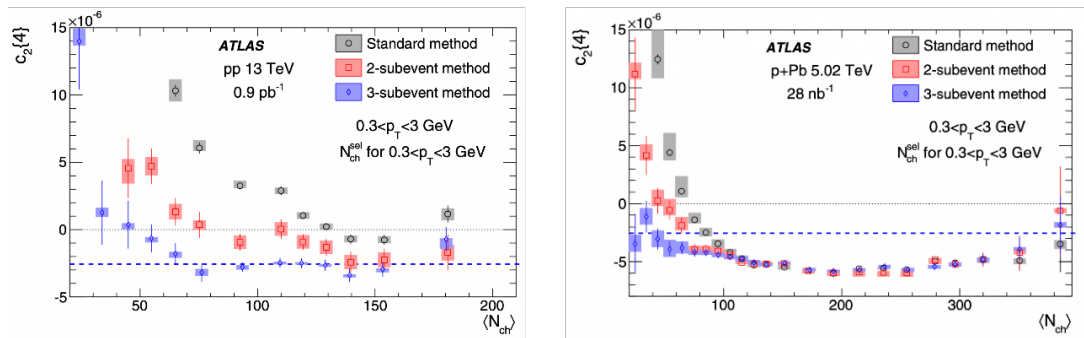
Figure 2.12: The 4-particle cumulant dependence on multiplicity measured in *pp* (left) and *p-Pb* (right) collisions obtained from standard and 2 and 3-subevent method [26].

25

Symmetric cumulants

The last measurement mentioned in this section is measurement of symmetric cumulants. Let us start with the ATLAS measurement of $SC_{2,4}$ dependence on multiplicity in pp (left) and p-Pb (right) collisions shown in the Fig. 2.13 using standard and subevent method. The values are positive for all methods and the trend is decreasing with $\langle N_{ch} \rangle$ for standard method and rather constant for subevent method in both collision systems. In pp collisions the values obtained from standard method are much larger than those from the subevent method, which is consistent with the expectation of larger non-flow contamination in standard method. Another decrease is observed between 2-subevent and 3-subevent method, which is linked to an insufficient suppression of non-flow correlations from di-jets in the 2-subevent method. In p-Pb collisions is observed a significant difference between standard and subevent method due to non-flow and almost no difference between subevent methods. The difference is notable in low-multiplicity events due to non-flow, but it is negligible in high-multiplicity collisions [17].

This result can be compared with the result of similar measurement of $SC_{2,4}$ in different collisions using 3-subevent method from ALICE experiment shown in the Fig. 2.14 (top). The values are positive in all multiplicity classes and compatible with previous ATLAS results in both pp and p-Pb collisions [22].

Figure 2.13: The measurement of $SC_{2,4}\{4\}$ in pp (left) and p-Pb (right) collisions using standard and subevent method [17].

Second measurement is dependence of $SC_{2,3}$ on multiplicity in pp (left) and p-Pb (right) collisions shown in the Fig. 2.15 using standard and subevent method at ATLAS experiment. The values in pp collisions obtained from standard method are positive in all multiplicity classes and the trend is descreasing with $\langle N_{ch} \rangle$. In contrast, the values obtained from subevent method are negative in all multiplicity classes and slightly more negative in low multiplicity events, which indicates strong non-flow contamination of the results obtained with the standard method. There is no significant difference between different subevent methods. Slightly different results
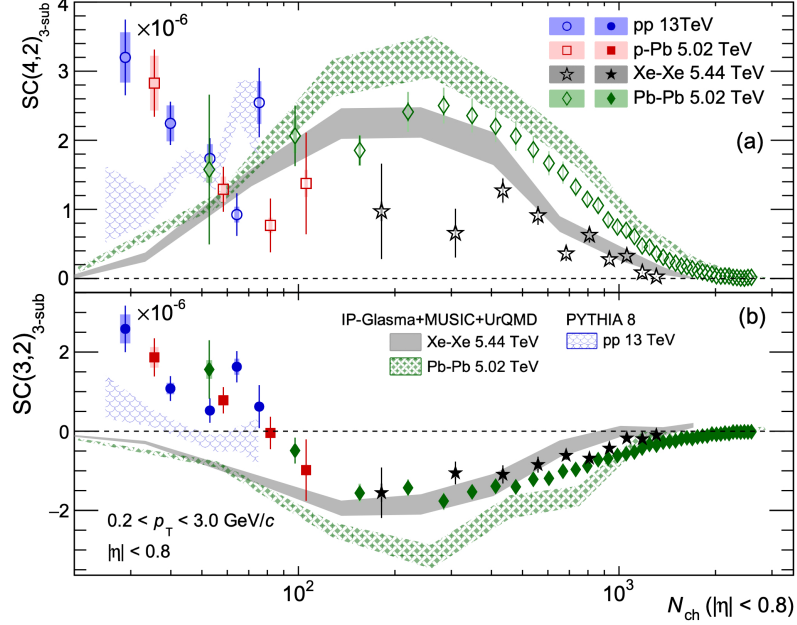
Figure 2.14: The measurement of $SC_{4,2}$ (a) and $SC_{3,2}$ (b) in *pp*, *p-Pb*, *Xe-Xe* and *Pb-Pb* collisions using 3-subevent method [22].

are observed in *p-Pb* collisions. At $\langle N_{ch} \rangle > 140$ there is no significant difference between standard and subevent method since all values remains negative and the trend is constant. This observation holds for $SC_{2,3}$ obtained from subevent method even in lower multiplicities, but the trend of $SC_{2,3}$ obtained from standard method is changing and the values of $SC_{2,3}$ changes sign around $\langle N_{ch} \rangle \sim 80$ and remains positive at low multiplicities, which is linked to non-flow contamination [17].

The result can be again compared with similar ALICE measurement shown in the Fig. 2.14 (bottom). In contrast to ATLAS measurement, we can observe here positive values of $SC_{2,3}$ obtained with 3-subevent method at $\langle N_{ch} \rangle < 80$ in both *pp* and *p-Pb* collisions [22]. Differences in measurements obtained using different detectors motivated us to do a detailed study of the influence of different acceptances of detectors on the flow measurements and most importantly on the suppression effect of the subevent method. The results of this study are presented in chapter 5.
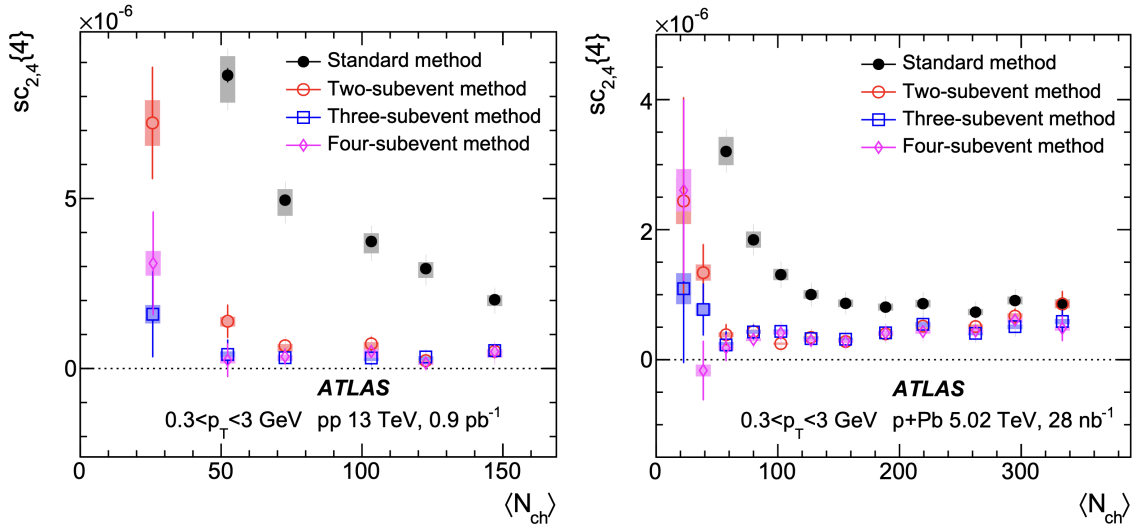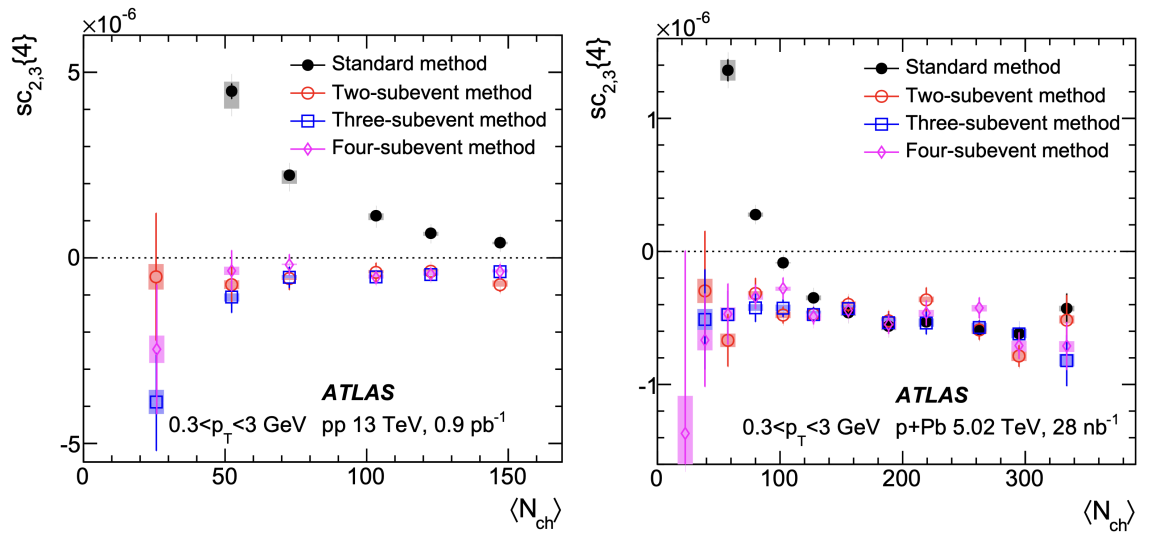
Figure 2.15: The measurement of $SC_{2,3}\{4\}$ in pp (left) and p-Pb (right) collisions using standard and subevent method [17].

Chapter 3

Method of azimuthal correlations

The computation of flow coefficients v_n turned out to be a bigger challenge. Imprecise determination of the symmetry plane angle Ψ from the definition of flow coefficients, event-by-event fluctuations introducing statistical inaccuracy and high computational requirements led to the most advanced and general method of flow computation denoted as Generic Framework (GF). This method also allows us to implement the subevent method for non-flow suppression in an efficient way. In the first part of this chapter the azimuthal correlations as a cornerstone of GF will be defined. Second part is dedicated to Generic Framework itself and in the final part the subevent method will be introduced and the computation in GF will be described in detail.

3.1 Azimuthal correlations of particles

As it was mentioned, computation of flow coefficients v_n from defining relation (2.2) turned out to be quite tricky, because determination of the symmetry plane angle Ψ from data for this purpose is imprecise. The solution is to replace the difference of particle azimuthal angle φ and symmetry plane angle Ψ in the definition with the difference of azimuthal angles of two particles and compute it for all possible pairs of particles. As an example let us to introduce relation for flow coefficients computed using two-particle correlation

$$\langle v_n^2 \rangle = \langle\langle \cos\left[n(\varphi_1 - \varphi_2)\right] \rangle\rangle \equiv \langle\langle 2 \rangle\rangle, \qquad (3.1)$$

where φ_1 and φ_2 are azimuthal angles of two particles in transverse plane. $\langle \cdot \rangle$ in the left expression denotes average over all collisions in particular centrality class and $\langle\langle \cdot \rangle\langle$ denotes average over all possible pairs of particles and all collisions of particular centrality. The resulting value of the flow coefficient obtained as a square root of (3.1) is then shifted from the value obtained from the definition due to a fluctuation of the flow coefficient around the mean value resulting from the event-by-event computation.

3.2 Generic Framework

3.2.1 Q-vector and m-particle correlations

Since the computation of flow coefficient using azimuthal correlations requires two nested for loops in an implementation, the method is becoming extremely computationally demanding with the increasing number of particles in an event. The solution is the most complex method for flow computation built on azimuthal correlations called Generic Framework [27]. This method provides fast and elegant way of computation of flow including implementation of the subevent method and in addition enables inclusion of detector efficiency using weights w. These weights can be considered as a compensation factors for detectors inefficiency in different azimuthal angles, e. g. less sensitive regions of detector has weight $w > 1$.

The essential building block of the GF is Q-vector defined by the relation [27]

$$Q_{n,p} = \sum_{k=1}^{M} w_k^p e^{in\varphi_k}, \tag{3.2}$$

where M is the total number of particles in particular sample, n is the order of flow coefficient and φ_k is respective azimuthal angle. It should be mentioned, that we now need only one for loop to calculate this vector and the definition (3.2) also implies a relation $Q_{-n,p} = Q_{n,p}^*$, which can be used for further simplification of computation.

We can write generic definition of the average m-particle correlation in harmonics $n_1, n_2, \ldots, n_m$ [27]

$$
\begin{aligned}
\langle m \rangle_{n_1,n_2,\ldots,n_m} &\equiv \\
\langle e^{i(n_1\varphi_1+n_2\varphi_2+\ldots+n_m\varphi_m)} \rangle &\equiv \frac{\displaystyle\sum_{\substack{k_1,k_2,\ldots,k_m=1 \\ k_1\neq k_2\neq\ldots\neq k_m}}^{M} w_{k_1} w_{k_2} \ldots w_{k_m} e^{i(n_1\varphi_{k_1}+n_2\varphi_{k_2}+\ldots+n_m\varphi_{k_m})}}{\displaystyle\sum_{\substack{k_1,k_2,\ldots,k_m=1 \\ k_1\neq k_2\neq\ldots\neq k_m}}^{M} w_{k_1} w_{k_2} \ldots w_{k_m}} \\
&= \frac{N\langle m \rangle_{n_1,n_2,\ldots,n_m}}{D\langle m \rangle_{n_1,n_2,\ldots,n_m}} = \frac{N\langle m \rangle_{n_1,n_2,\ldots,n_m}}{N\langle m \rangle_{0,0,\ldots,0}}.
\end{aligned}
\tag{3.3}
$$

Using the definition of Q-vector (3.2) we can formulate particular formulas of numerator $N\langle m \rangle_{n_1,n_2,\ldots,n_m}$ for two-particle (3.4), three-particle (3.5) and four-particle (3.6) correlation [27]

$$N\langle 2 \rangle_{n_1,n_2} = Q_{n_1,1} Q_{n_2,1} - Q_{n_1+n_2,2}, \tag{3.4}$$

$$
\begin{aligned}
N\langle 3 \rangle_{n_1,n_2,n_3} &= Q_{n_1,1} Q_{n_2,1} Q_{n_3,1} - Q_{n_1+n_2,2} Q_{n_3,1} - Q_{n_2,1} Q_{n_1+n_3,2} \\
&\quad - Q_{n_1,1} Q_{n_2+n_3,2} + 2Q_{n_1+n_2+n_3,3},
\end{aligned}
\tag{3.5}
$$

$$N\langle 4\rangle_{n_1,n_2,n_3,n_4} = Q_{n_1,1}Q_{n_2,1}Q_{n_3,1}Q_{n_4,1} - Q_{n_1+n_2,2}Q_{n_3,1}Q_{n_4,1}$$
$$-Q_{n_2,1}Q_{n_1+n_3,2}Q_{n_4,1} - Q_{n_1,1}Q_{n_2+n_3,2}Q_{n_4,1} + 2Q_{n_1+n_2+n_3,3}Q_{n_4,1}$$
$$-Q_{n_2,1}Q_{n_3,1}Q_{n_1+n_4,2} + Q_{n_2+n_3,2}Q_{n_1+n_4,2} - Q_{n_1,1}Q_{n_3,1}Q_{n_2+n_4,2}$$
$$+Q_{n_1+n_3,2}Q_{n_2+n_4,2} + 2Q_{n_3,1}Q_{n_1+n_2+n_4,3} - Q_{n_1,1}Q_{n_2,1}Q_{n_3+n_4,2}$$
$$+Q_{n_1+n_2,2}Q_{n_3+n_4,2} + 2Q_{n_2,1}Q_{n_1+n_3+n_4,3}$$
$$+2Q_{n_1,1}Q_{n_2+n_3+n_4,3} - 6Q_{n_1+n_2+n_3+n_4,4}. \tag{3.6}$$

As we have seen in the previous equations, an auto-correlation term is always involved in relations due to overlapping selection of particles.

3.2.2 Cumulants and flow coefficients

Flow coefficients v_n can be calculated from the m-particle correlations using the same harmonic $n_1 = n_2 = \ldots = n_m \equiv n$. Firstly, m-particle correlations averaged over all pairs of particles and events defined in previous section are used for computation of the m-particle cumulants $c_n\{m\}$, e.g. the formulas for 2-particle and 4-particle cumulants are shown in Eq. (3.7) and (3.8)

$$c_n\{2\} = \langle\langle 2\rangle\rangle_{n,-n}, \tag{3.7}$$

$$c_n\{4\} = \langle\langle 4\rangle\rangle_{n,n,-n,-n} - 2 \cdot \langle\langle 2\rangle\rangle_{n,-n}^2, \tag{3.8}$$

where numbers in brackets $\{\cdot\}$ represents number of particles used for correlation. As we can see 2-particle cumulant is directly equal to 2-particle correlation. On the other hand, in order to obtain 4-particle cumulant, contributions from 2-particle correlation have to be subtracted. Relations for 6, 8, or more-particle cumulants are becoming progressively more complicated because the lower-order contributions have to be subtracted in each case, and therefore the explicit forms are not given in this work.

The flow coefficients v_n are then obtained from the cumulants using Eqs. (3.9) and (3.10):

$$v_n\{2\} = \sqrt{c_n\{2\}}, \tag{3.9}$$

$$v_n\{4\} = \sqrt[4]{-c_n\{4\}}. \tag{3.10}$$

We should remark here that the value of flow coefficient $v_n\{4\}$ obtained from 4-particle correlation is real only under the condition of negative 4-particle cumulant.

3.2.3 Symmetric cumulants

The correlation between two orders of flow coefficients v_i and v_j can be measured using Symmetric cumulants defined as

$$SC(i,j) = \langle v_i^2 \cdot v_j^2 \rangle - \langle v_i^2 \rangle \cdot \langle v_j^2 \rangle, \tag{3.11}$$

where $\langle \cdot \rangle$ denotes average over events. No correlation between v_i and v_j leads to zero value of symmetric cumulant. On the other hand, a non-zero value of $SC(i,j)$ indicates the existence of correlation.

Using different harmonics $i \neq j$ of m-particle correlation allows us to calculate the symmetric cumulant in following way

$$SC(i,j) = \langle\langle 4 \rangle\rangle_{i,j,-i,-j} - \langle\langle 2 \rangle\rangle_{i,-i} \cdot \langle\langle 2 \rangle\rangle_{j,-j}, \tag{3.12}$$

where $\langle\langle \cdot \rangle\rangle$ represents average over all pairs of particles and events.

3.3 Suppression of non-flow contamination

We have defined flow as global long-range correlations of particles, but the derivation of flow from GF using cumulants does not exclude short-range correlations by design. Short-range correlations, which are correlations between particles coming from jets and decays of heavy particles, increasing the overall signal. In order to measure flow without background, we need to get rid of this contamination. The following section is devoted to two ways how to suppress non-flow, which can be used separately or together.

3.3.1 Multiparticle correlations

The more particles we take into the correlation, the lower the contribution of non-flow is, e.g. 4-particle correlation is less sensitive to non-flow than 2-particle correlation. The 2-particle correlation is calculated from azimuthal angles of all possible pairs. The 4-particle correlation can be similarly obtained as an average of correlations of all possible quadruplets of particles. Since the probability, that all particles in a quadruplet come from a single jet cone or a single decay, is lower than in the case of two particles and correlations of lower orders are subtracted in computation of appropriate cumulants as we have seen in section 3.2.2, we can conclude that the resulting multiparticle cumulants will be less sensitive to non-flow than cumulants obtained from the 2-particle correlation.

3.3.2 Subevent method

The more sophisticated method of non-flow background is called subevent method. The method consists in dividing the η-acceptance of the detector into two or more

regions called subevents separated by some space called η-gap and taking into correlation only particles from different subevents [28] as it will be described in detail in the following sections. The particles from the η-gap are then not taken into account at all. In this way we can isolate jet cone or decay in one of subevents and therefore we no longer calculate correlations between particles from a single cone or decay. The correlations of particles from jets located in central rapidity are completely removed thanks to the η-gap.

2-particle correlation

The simplest example of using the subevent method is calculation of two-particle correlation. The η-acceptance of the detector is divided into two subevents separated by η-gap and according to the previous section first particle is chosen from subevent A and second one from subevent B. The situation is illustrated in Fig. 3.1. The relation for 2-particle correlation with 2-subevent method is [28]

$$c_n\{2\}_{2-sub} = \langle\langle 2 \rangle\rangle_{n,AB} = \langle\langle e^{in(\varphi_A - \varphi_B)} \rangle\rangle. \tag{3.13}$$

Thanks to this method, correlations from decays and jets are suppressed effectively. The enlargement of η-gap leads to exclusion of particles situated in central rapidity region, which means that non-flow correlations from jets in this region are suppressed, but at the same time the statistical uncertainty of correlation is increased.
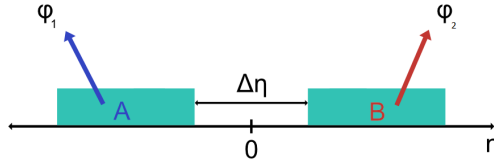
Figure 3.1: The method of 2 subevents separated by *eta*-gap for two-particle correlations.

4-particle correlation

The non-flow in measurements of 4-particle cumulant, which is by design less sensitive to this background, can be reduced by 2-subevent and 3-subevent method with various configurations. In the basic configuration of 2-subevent method are taken into correlation 2 particles from subevent A and 2 particles from subevent B, which is illustrated in Fig. 3.2. The 4-particle cumulant is then obtained from 4-particle and 2-particle correlations both calculated with 2-subevent method as follows [28]

$$c_n\{4\}_{2-sub} = \langle\langle 4 \rangle\rangle_{n,AB}^{1+2,3+4} - \langle\langle 2 \rangle\rangle_{n,AB}^{1,3} \cdot \langle\langle 2 \rangle\rangle_{n,AB}^{2,4}$$
$$-\langle\langle 2 \rangle\rangle_{n,AB}^{1,4} \cdot \langle\langle 2 \rangle\rangle_{n,AB}^{2,3} = \langle\langle 4 \rangle\rangle_{n,AB} - 2 \cdot \langle\langle 2 \rangle\rangle_{n,AB}^2. \tag{3.14}$$

The numbers in the superscript denote the way how particles in correlation were chosen from subevents, e.g. the expression $\langle\langle 2 \rangle\rangle_{n,AB}^{1,3}$ denotes 2-particle correlation of particle 1 from subevent A and particle 3 from subevent B (marked according to Fig. 3.2). Since all particles are correlated with all other, there is no difference between 2-particle correlations $\langle\langle 2 \rangle\rangle_{n,AB}^{1,3}$ and $\langle\langle 2 \rangle\rangle_{n,AB}^{2,4}$. The 2-subevent method applied in measurements of 4-particle cumulant is expected to lead to even better suppression of non-flow background.
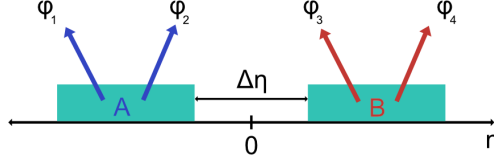
Figure 3.2: The method of 2 subevents separated by η-gap for four-particle correlations.

Since 4 particles are now used for correlation instead of 2, the η-acceptance of detector can be divided into three subevents separated by 2 η-gaps. The situation is illustrated in Fig. 3.3. There are several ways how to pick 4 particles from 3 subevents, but the most common approach is to take two particles from the middle subevent A, one particle from the left subevent B and one particle from the right subevent C. Alternatively, we can pick two particles from subevent B or C. The final formula for 4-particle cumulant is a bit more complicated, because there are two distinct ways how to choose 2 pairs from 3 subevents [28]

$$
\begin{aligned}
c_n\{4\}_{3-sub} &= \langle\langle 4 \rangle\rangle_{n,ABC}^{1+2,3,4} - \langle\langle 2 \rangle\rangle_{n,AB}^{1,3} \cdot \langle\langle 2 \rangle\rangle_{n,AC}^{2,4} \\
-\langle\langle 2 \rangle\rangle_{n,AC}^{1,4} \cdot \langle\langle 2 \rangle\rangle_{n,AB}^{2,3} &= \langle\langle 4 \rangle\rangle_{n,ABC} - 2 \cdot \langle\langle 2 \rangle\rangle_{n,AB} \cdot \langle\langle 2 \rangle\rangle_{n,AC}.
\end{aligned}
\tag{3.15}
$$

The 3-subevent method is useful especially in events with two jet cones created in opposite directions, because the 2-subevent method suppresses non-flow correlations within one jet cone, but the 3-subevent method suppresses also correlations between jet cones in most cases. Of course, the suppression effect depends on the jet width and its orientation.

Subevent method in the Generic Framework

The calculation of cumulants with the subevent method can be easily implemented in the Generic Framework, where Q-vectors are used for computation of correlations. Q-vectors are usually computed from all particles produced in particular event, but in the case of the subevent method, Q-vectors are calculated only from particles situated in particular subevent. The relation for 2-particle correlation, which can be compared with the original form in Eq. (3.4), then can be rewritten in the following way
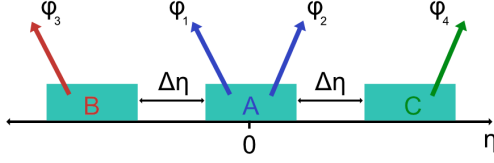
Figure 3.3: The method of 3 subevents separated by η-gap for four-particle correlations.

$$N\langle 2\rangle_{n_1,n_2} = Q^A_{n_1,1}Q^B_{n_2,1}, \tag{3.16}$$

where Q^A and Q^B are Q-vectors computed from particles in subevent A and subevent B, respectively. There is no further need to subtract auto-correlation term, because there is no overlap between particles from different subevents. Four-particle correlation with the 2-subevent method can be rewritten in similar way

$$\begin{aligned} N\langle 4\rangle_{n_1,n_2,n_3,n_4} = {} & Q^A_{n_1,1}Q^A_{n_2,1}Q^B_{n_3,1}Q^B_{n_4,1} - Q^A_{n_1+n_2,2}Q^B_{n_3,1}Q^B_{n_4,1} \\ & -Q^A_{n_1,1}Q^A_{n_2,1}Q^B_{n_3+n_4,2} + Q^A_{n_1+n_2,2}Q^B_{n_3+n_4,2}. \end{aligned} \tag{3.17}$$

Compared to (3.6), 11 auto-correlation terms were removed and even more terms are removed in the following relation with the 3-subevent method

$$N\langle 4\rangle_{n_1,n_2,n_3,n_4} = Q^A_{n_1,1}Q^A_{n_2,1}Q^B_{n_3,1}Q^C_{n_4,1} - Q^A_{n_1+n_2,2}Q^B_{n_3,1}Q^C_{n_4,1}. \tag{3.18}$$

Configurations of the 3-subevent method

In the final section of this chapter, let us remark that the η-acceptance of a detector can be divided into three subevents in many ways. There are two different layouts, which are currently used. The first one considers all three subevents of the same size and since it was firstly used at ATLAS experiment, let us denote it here as AT-LAS configuration. The second one, used for the first time at ALICE experiment, considers the middle subevent twice as large as the others and will be futher denoted as ALICE configuration. The motivation behind the ALICE configuration is as follows. To calculate the 4-particle correlation, we usually take one particle from the left subevent, one from the right subevent, and two particles from the middle subevent. To have a sufficiently large number of particles in each subevent, it is convenient to take the middle subevent double as the others.

The comparison of results obtained using these two configurations is one of the main goals of this diploma thesis.

Chapter 4

PYTHIA 8 and FastJet

In order to study the method of multiparticle cumulants for anisotropic flow computation we use PYTHIA model [29], which enables us to simulate a huge amount of high-energy collisions of specific parameters using current theoretical models. Artificial origin of our dataset allows us to compare how different acceptances of detectors affect a measurement of flow or to determine which configuration of the subevent method used for non-flow suppression is best for reconstruction of introduced flow signal. Lastly, it enables us to easily reduce statistical uncertainties by generating enough events, which is extremely important in studies of collective behaviour in collisions of small systems. PYTHIA is a purely non-flow model, which means that we should not expect results directly comparable to experimental results. But since we only want to study non-flow contamination depending on the different detector acceptances or layouts of the subevent method, this model is perfectly suitable in our case.

In the second part of this thesis we study how collimated sprays of particles called jets affect the method of multiparticle cumulants. Jets form a large part of non-flow background in our measurements and therefore it is crucial to study how the subevent method suppress this type of non-flow correlations. The FastJet software package is used to identify the particles that are part of the jet.

The first part of the following chapter is devoted to short introduction to PYTHIA 8 and description of the workflow used in our analysis. In the second part we introduce basic jet terminology and briefly describe how FastJet works.

4.1   Introduction to PYTHIA 8

The PYTHIA is a general purpose Monte Carlo event simulator based on a coherent set of physical models describing a large number of physics phenomena such as hard and soft interactions, parton showers, fragmentation or decays [29]. The current theoretical models are used to construct a set of final particles with their properties (momentum, angles of production, mass etc.) from randomly chosen initial conditions using selected processes briefly described in [29]. Firstly, primary interactions

of incoming particles are modeled according to the perturbative QCD. Furthermore, interactions of secondary partons and interactions of beam remnants are modeled. Finally, the modeling of hadronization process and particle decays leads to set of final particles.

Many currently known processes are already implemented in PYTHIA and even more processes are being constantly developed. The most recent version of the simulator is PYTHIA 8.3 including models of hard processes (e.g. QCD processes, EW processes, top production, Higgs processes, SUSY processes), soft processes (elastic, diffractive and non-diffractive topologies), different parton distribution functions, parton showers, multiparton interactions, interactions of beam remnants, colour reconnection, hadronization (Lund string fragmentation framework) and particle decays [29].

Since PYTHIA is a purely non-flow driven model, no collective behaviour can be observed in generated events. Yet we can study suppression of non-flow created by the subevent method or we can introduce some artificial flow signal to the generated dataset and investigate which configuration of the subevent method reconstruct the signal most effectively.

The simulator is limited by two allowed collision topologies (hadron-hadron and lepton-lepton) and a minimum centre-of-mass collision energy equal to 10 GeV. Possible collision topologies can be extended using models such as *Angantyr* [30] combining several nucleon-nucleon collisions into a single heavy-ion collision. Another limitation of PYTHIA is the absence of simulation of the interaction of the created particles with the detector material, which is well suited for various studies where the detector inefficiencies or other experimental aspects do not need to be taken into consideration.

4.1.1 Workflow

PYTHIA is typically used as an imported library in a generating script written in C++ or Python (the following examples follow C++ syntax). Firstly, PYTHIA is usually declared by *Pythia pythia* command followed by collision settings defined either parameter by parameter in a form *pythia.readString(PARAMETER = VALUE)* or from an external text file loaded by command *pythia.readFile(FILE PATH)*. All parameters are listed on the website *pythia.org/latest-manual* divided into several categories - beam parameters (e.g. PDG ID codes of incoming particles or collision CMS energy), soft processes, hard processes, diffraction, hadronization and so on. Another option is to use one of the predefined tunes (sets of parameters), which have been created within the PYTHIA group or by different collaborations. Finally, PYTHIA generator is initialized using user defined parameters by *pythia.init()* and events are generated in a for-loop by command *pythia.next()*. The output of each generative run is an object containing final particles with their properties (full list is availiable in [29]), which can be stored in a ROOT object (e.g. TTree or TNtuple) and saved as a ROOT file for following analysis.

4.2 Jets

Jets are collimated sprays of hadrons resulting from fragmentation of high-energy scattered partons generated in initial stages of the collision. As we have already mentioned, in the extreme conditions created after a relativistic hadron collision, the scattered partons can move freely and produce radiation in the form of gluons and quark-antiquark pairs in the process called fragmentation. Partons are then bound to hadrons, which move in the direction of original partons and reflects their properties. In result, jets form characteristic cone structure, where the original parton is located at the tip and the base of the cone contains final particles recorded in detectors.

4.2.1 Jet algorithms

In order to determine, which final particles are part of a jet, we use algorithms designed to reconstruct energy and direction of the original parton. These algorithms can be divided into two groups - cone and sequential. One of the most important requirement for all jet algorithms is infrared and collinear safety, which means that the jet reconstructed by the algorithm should not change by adding soft particle radiated by the original parton or by splitting the original parton into two collinear partons.

The most important for the purposes of this thesis are sequential algorithms based on selecting one initial particle and then adding closest particles until the entire jet is formed. This class includes k_t and anti-k_t algorithms, which are used in the context of this thesis and will be described in following sections.

k_t algorithm

The jet reconstruction using k_t algorithm can be divided into three steps [31]:

1. For each pair of particles i, j the d_{ij} distance is calculated according to

$$d_{ij} = \frac{\min(p_{T_i}^2, p_{T_j}^2)\Delta R_{ij}^2}{R^2}, \tag{4.1}$$

   with $\Delta R_{ij}^2 = (y_i - y_j)^2 + (\varphi_i - \varphi_j)^2$, where p_{T_i}, y_i and φ_i are the transverse momentum, rapidity and azimuthal angle of the particle i. R is jet-radius parameter and the beam distance for each parton can be determined as $d_{iB} = p_{T_i}^2$.

2. Then the minimum d_{min} of all the d_{ij} and d_{iB} is found. If $d_{min} = d_{ij}$, particles i and j are merged into a single particle by summing their four-momenta. If $d_{min} = d_{iB}$, particle i is considered as a final jet and removed from the list.

3. The process is repeated until no particles are left.

anti-k_t algorithm

The anti-k_t algorithm is identical to the k_t algorithm except the definitions of distances d_{ij} and d_{iB}

$$d_{ij} = \frac{\min\left(\frac{1}{p_{T_i}^2}, \frac{1}{p_{T_j}^2}\right)\Delta R_{ij}^2}{R^2},$$

(4.2)

$$d_{iB} = \frac{1}{p_{T_i}^2}.$$

(4.3)

Unlike the previous algorithm, in this case clustering starts from the particles with high p_T. Since the algorithm behaves like a perfect cone algorithm, it is most suitable for jet reconstruction [31].

4.2.2   FastJet

FastJet is a C++ library providing implementations of many clustering algorithms for jet finding in *pp* and e^+e^- collisions. Except for the jet reconstruction algorithms, FastJet provides several advanced tools that are custom made for jet finding purposes. The most important classes are *fastjet::PseudoJet, fastjet::JetDefinition* and *fastjet::ClusterSequence.*

The *PseudoJet* object is used to store jets and input particles and can be created by specifying four-momentum of jet or particle in the following constructor *PseudoJet (double px, double py, double pz, double E)*. The appropriate components can be then accessed by predefined functions (e.g. *rap()* returns rapidity, *m()* returns invariant mass). In the constructor of *JetDefinition*, the jet algorithm (e.g. k_t or anti-k_t), parameters (e.g. radius R), the recombination scheme for 4-momenta of *PseudoJets* and the algorithm strategy must be specified. For jet clustering, a *ClusterSequence* object is defined by specifying input particles (a vector of *PseudoJets*) and *JetDefinition*. More detailed information along with a list of implemented algorithms is given in [31].

Chapter 5

Study of the multiparticle cumulant method

The following chapter is dedicated to the first objective of this diploma thesis, namely the study of the multiparticle cumulant method with an emphasis on the suppression of non-flow background in collisions of small systems. In order to complete this task the dataset of 2 billion pp collisions was generated in PYTHIA model. The main focus is given to the study of the subevent method and its configurations applied on the dataset with cuts according to ALICE and ATLAS acceptances.

The first part of this chapter is devoted to the dataset, selected PYTHIA parameters and basic overview of the analysis workflow. The second section introduces the concept of injected flow, which is used in the third part of this chapter with results.

5.1 Dataset and analysis workflow

5.1.1 PYTHIA settings

The dataset of 2 billion pp collisions was generated in PYTHIA 8.303 using the configuration used by the ALICE collaboration. The parameters changed from the default settings are the following:

Beams:eCM = 13000.
SoftQCD:inelastic = on
ParticleDecays:limitTau0 = on
Random:setSeed = on

These parameters together with the default values of others set up configuration, in which pp collisions in the default tune called *Monash 2013* [32] at the center-of-mass energy $\sqrt{s} = 13\,\mathrm{TeV}$ with enabled soft inelastic and disabled soft elastic processes are generated using manual seeding.
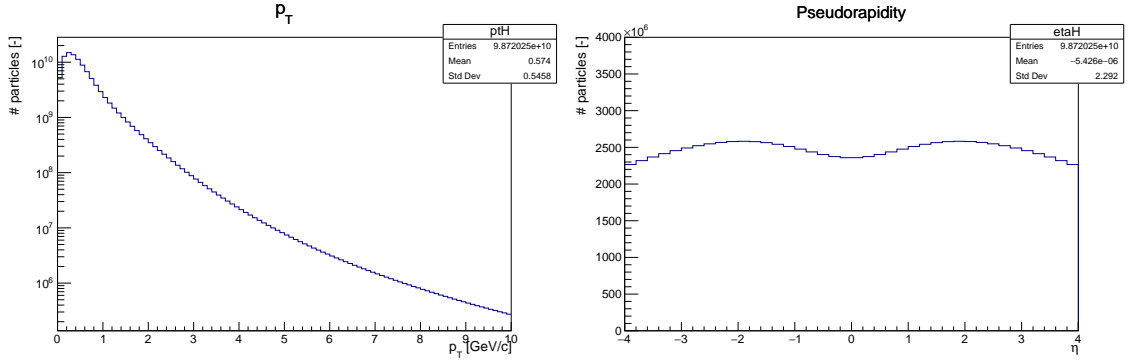
Figure 5.1: Distributions of the transverse momenta p_T and the pseudorapidities η of the particles in the dataset generated in PYTHIA.
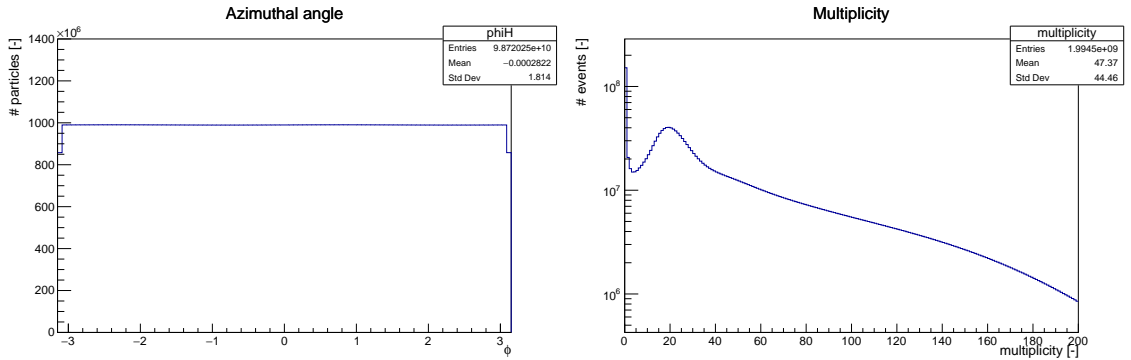
Figure 5.2: Distribution of azimuthal angles ϕ of the particles in the dataset generated in PYTHIA (left) and histogram of the multiplicities of generated events (right).

5.1.2 Running simulation and storing output

The entire dataset was generated in 4000 separate jobs in the computer cluster of the Department of Physics at the FNSPE CTU. The output of each job is a ROOT file containing a TTree with a list of produced particles with selected properties (transverse momentum, pseudorapidity, charge, azimuthal angle and PDG code). The seed was manually set in the range of 1-4000, allowing us to reproduce the same dataset in the future.

Distributions of the transverse momenta p_T and the pseudorapidities η of the particles in the generated dataset are in Fig. 5.1. Only particles with $|\eta| < 4$ were stored in TTrees in our case, since it is a sufficient range for our further analysis according to the ALICE and ATLAS η-acceptances. Distribution of the azimuthal angles ϕ of the particles in the generated dataset are in the left panel of Fig. 5.2 and histogram of multiplicities of generated events in the right panel of Fig. 5.2.

5.1.3   Analysis workflow

In order to study in detail the multiparticle cumulant method with different settings of the subevent method, we developed from scratch our own analysis code based on the Generic Framework described in 3.2, despite other already existing implementations.

The steps of our analysis workflow are following:

1. Load a ROOT output file containing a list of created particles with its properties and apply p_T and η cuts according to the acceptance of selected detector. Compute required Q-vectors in a FOR loop over all particles, compute desired m-particle correlations $\langle m \rangle$ averaged over particles (number of particles in the correlation, order of the correlation and the subevent method are specified as parameters) and fill them into TProfiles saved as a ROOT file. The previous three steps (Q-vectors, correlations and saving to TProfiles) are executed in an another FOR loop over all events in the data file containing 500 000 collisions. The output of this step is then one file (containing TProfiles with correlations averaged over particles and 500 000 events) per one data file.

2. Merge particular TProfiles containing correlations computed from all data files into one set of final TProfiles (containing correlations $\langle\langle m \rangle\rangle$ averaged over particles and 2 billion events) and save it as a new ROOT file. This step is done by the ROOT command *hadd all.root *.root.*

3. Load the ROOT file with all computed correlations created in the previous step, compute desired cumulants according to the equations from section 3.2.2 and fill them into TProfiles saved as a ROOT file.

4. Load the output files and plot desired results.

Two notes should be made here. Firstly, the entire data analysis process is done in multiplicity unit bins. One of the reasons for this approach is the computation of 4-particle cumulant $c_2\{4\}$, where the 2-particle correlation is subtracted from the 4-particle correlation according to (3.8). The values of these correlations used in the calculation of the 4-particle cumulant should be obtained from the same events, i.e. events with the same multiplicity, and the computation in unit bins allows us to do this. Rebinning is then done in the very last step of the process. In order to be able to easily compare results obtained with different detector acceptances bin by bin, the multiplicity of an event is calculated consistently according to ALICE acceptance in all following measurements. Secondly, the errors of the cumulants are computed in a specific way. Collisions in each set of 500 000 events are randomly divided into ten subsets at the start of the correlation computation. Correlations and cumulants are then computed for each of these ten subsets separately. The resulting value and error of particular cumulant are obtained from cumulants computed in separate subsets (considering them as independent measurements).

5.2 Injected flow

As it was mentioned PYTHIA is purely non-flow model, but flow signal can be introduced into PYTHIA manually by modifying the φ-distribution of particles. The motivation of this process is to study which configuration of the subevent method reconstructs introduced flow signal best and whether non-flow can be sufficiently suppressed using limited acceptance of ALICE.

In our case the injection method using the Newton–Raphson numerical method proposed in [33] is used. Let us assume that only elliptic flow v_2 is present. Then the core equation of the method is relation for modification of φ of particle

$$\varphi_0 \rightarrow \varphi = \varphi_0 - \tilde{v}_2 \sin[2(\varphi - \Psi_{RP})], \tag{5.1}$$

where φ_0 is the original azimuthal angle of particle, $\tilde{v}_2$ is injected flow signal and Ψ_{RP} is the reaction plane angle in the transverse plane, which is randomly chosen from uniform distribution in the range $0 - 2\pi$. Since the equation (5.1) is transcendental, the solution for φ should be found numerically and at this point, the Newton–Raphson method is used [33].

5.3 Results

The most important results are presented in the following section, which is divided into three parts - comparison of ALICE and ATLAS acceptances, study of different configurations of the 3-subevent method and reconstruction of injected flow signal in the context of the previous two parts. More results can be found in Appendix.

5.3.1 Comparison of ALICE and ATLAS acceptances in the multiparticle cumulant method

The difference between η-acceptances of ALICE and ATLAS detectors could have significant impact on flow measurements. Since the ATLAS acceptance is considerably wider than the ALICE acceptance, the ratio of long-range and short-range correlations is expected to be noticeably different for the two detectors. The wider ATLAS acceptance also enables us to choose the layout of the subevent method more flexibly, e.g. making possible measurements with very large η-gaps. Lastly, as it was mentioned in section 2.2.2, the measurements of symmetric cumulants in low-multiplicity collisions of small systems differ significantly for ALICE and ATLAS acceptances. These observations and expectations motivated our investigation of how different acceptances of detectors affect flow measurements. More specifically, we would try to answer the question of whether the difference in the previously mentioned measurement originates from the limited acceptance of ALICE (because non-flow cannot be sufficiently suppressed) or the large acceptance of ATLAS (including long-range non-flow background and decorrelations to measurements).

The p_T-acceptance of both ALICE and ATLAS detectors was chosen for all our following measurements to be $0.3 < p_T < 3.0\,\text{GeV/c}$, as it is the usual range in which flow is measured. The η-acceptances of ALICE and ATLAS are considered to be $|\eta| < 0.8$ and $|\eta| < 2.5$, respectively.

The left panel of Fig. 5.3 is devoted to the measurement of dependence of 2-particle cumulant $c_2\{2\}$ on multiplicity in pp collisions at the centre-of-mass energy $\sqrt{s} = 13\,\text{TeV}$. The comparison of results obtained using ALICE and ATLAS acceptances with 2-subevent method can be observed. The η-gaps used in this case are $\Delta\eta = 0, 0.2, 0.4$. Both ALICE and ATLAS cumulants indicate significant dependence on multiplicity. As expected, the subevent method provides a suppression of non-flow background, which is more significant for larger η-gaps. Regardless of the suppression, the multiplicity dependence of the cumulants remains present. It is a direct consequence of the fact that PYTHIA is purely non-flow model, and therefore only the non-flow background is suppressed by the subevent method without revealing any other phenomenon. The apparent change of the trend in ALICE measurement in bins 70-100 is caused by statistical fluctuations due to a small number of generated high-multiplicity collisions.

The difference between multiplicity dependencies of $c_2\{2\}$ for different acceptances is clear. The limited η-acceptance of ALICE situated in the central rapidity region leads to a significant dominance of short-range correlations over long-range correlations due to the generally lower $\Delta\eta$ between particles. As a result, the non-flow background is stronger and the values of cumulants are higher as we can see in Fig. 5.3 (left). Both enlargements (from 0 to 0.2, from 0.2 to 0.4) of the η-gap in the 2-subevent method lead to an increase in non-flow suppression of $\sim 15\,\%$ in the ALICE case and $\sim 11\,\%$ in the ATLAS case. As we can see in Fig. A.1 in Appendix, not even large η-gap $\Delta\eta = 1.0$ leads to complete suppression of non-flow in ALICE measurement due to background correlations from di-jets, which are handled more effectively in 3-subevent method. On the other hand the enlargement of η-gap to $\Delta\eta = 2.0$ in ATLAS measurement leads to values of cumulant compatible with zero in high-multiplicity events.

In the right panel of Fig. 5.3 the measurement of dependence of 4-particle cumulant $c_2\{4\}$ on multiplicity in pp collisions at the same energy can be observed. Similarly to the previous measurement the results obtained using ALICE and ATLAS acceptances with 2 and 3-subevent method with η-gap $\Delta\eta = 0$ can be compared. Bin 0-10 is empty because of large statistical fluctuations associated with the fact, that there are only few particles in those low-multiplicity events, and therefore it is imprecise or even impossible to compute correlation out of four particles with an η-gap requirement. Bins 80-100 are empty due to statistical fluctuations caused by low number of high-multiplicity events. The overall trend is decreasing for both ALICE and ATLAS acceptances and the 3-subevent method provides additional suppression of non-flow, which is most significant in low-multiplicity events.

The transition from the 2-subevent method to the 3-subevent method is more apparent in ATLAS measurement, where specifically for low-multiplicity events, the 3-subevent method provides a huge improvement in non-flow suppression. In ALICE results compatibility of cumulant with zero is achieved in bins 60-80 and 50-80
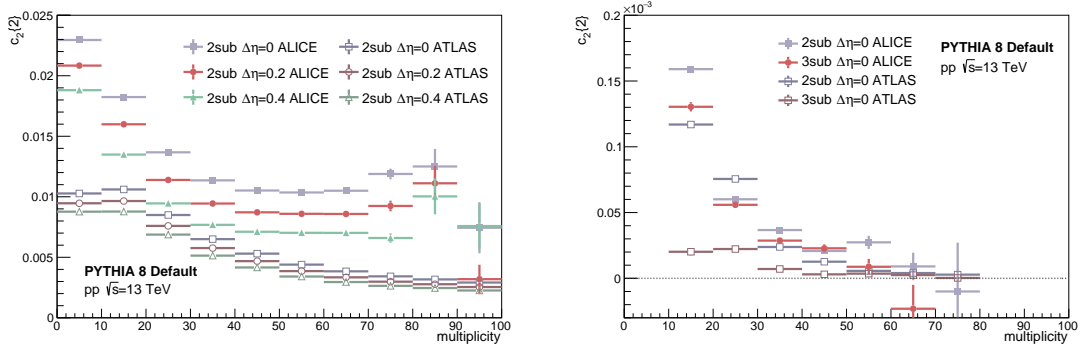
Figure 5.3: The comparison of two-particle cumulant $c_2\{2\}$ (left) and four-particle cumulant $c_2\{4\}$ (right) dependencies on multiplicity of ATLAS and ALICE acceptances using 2-subevent method with $\Delta\eta = 0, 0.2, 0.4$ and 2 and 3-subevent method with $\Delta\eta = 0$, respectively.

using 2 and 3-subevent method, respectively. In ATLAS results the compatibility is reached already in bins 50-80 and 30-80 using 2 and 3-subevent method, respectively. The difference probably comes from insufficient η-separation between particles from jets in ALICE measurement. It is more likely to place particles from one jet cone into two different subevents with the smaller η-acceptance of ALICE. This can also occur in ATLAS measurement, but there are many well-separated particles that are long-range correlated.

5.3.2 Study of different configurations of 3-subevent method

As it was mentioned in section 3.3.2, ALICE and ATLAS experiments use different layouts of subevents in the 3-subevent method and therefore we would like to study, which layout is more successful in non-flow suppression. The results can be then further compared for ALICE and ATLAS acceptances. Let us denote here the layout in which all subevents are of the same size as *(1-1-1)* and the other layout, considering the middle subevent twice as large as the others, as *(1-2-1)*. More details on these two layouts are given in section 3.3.2. The acceptances of detectors are considered same as in the previous section.

The dependence of four-particle cumulant $c_2\{4\}$ on multiplicity in *pp* collisions at the centre-of-mass energy $\sqrt{s} = 13\,\text{TeV}$ using ALICE acceptance is in Fig. 5.4 (left). The 3-subevent method with η-gaps $\Delta\eta = 0$ and two layouts of subevents was used. Bins 0-10 and 70-100 are empty due to reasons mentioned in the previous section. Results obtained with both layouts follow same decreasing trend reaching values approximately compatible with zero in bins 50-70, but the statistical uncertainties are large in those events, so the result is not precise. The values of cumulant obtained with (1-2-1) layout are generally lower than those obtained with (1-1-1) layout. The additional enlargement of the η-gap is significantly more apparent in (1-1-1) configuration, as it can be seen in Fig. A.2 in Appendix. On the other hand, in (1-2-1) layout the difference is almost negligible. Together it indicates stronger
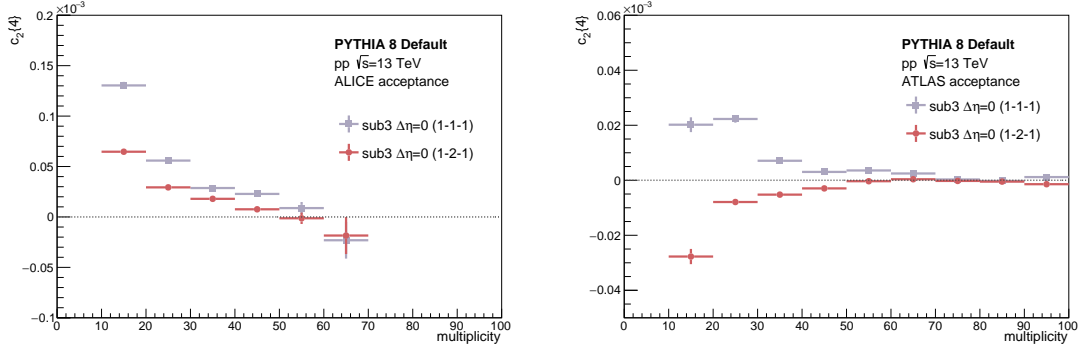
Figure 5.4: The four-particle cumulant $c_2\{4\}$ dependency on multiplicity of ALICE (left) and ATLAS (right) acceptances using 3-subevent method with $\Delta\eta = 0$ and two different configurations (1-1-1) and (1-2-1) described in the text.

non-flow background in (1-1-1) configuration that could be related to the following assumption. The larger middle subevent in (1-2-1) layout may lead to a higher probability of separation of a single jet cone in the middle subevent and a larger ratio of long-range to short-range correlations due to a larger η-separation between two edge particles from outer and middle subevents.

The same measurement with ATLAS acceptance is in the right panel of Fig. 5.4. The first bin is empty for the same reasons as in the previous case. We can observe significant difference between trends of cumulant values obtained with two different layouts in this case. Firstly, (1-1-1) layout leads to decreasing trend with an exception in bins 10-30, where the statistical fluctuations are strong. The effect of larger η-gap is apparent only in bins 10-40, where $\Delta\eta = 0.2$ provides lower values of cumulant. The 4-particle cumulant is approximately compatible with zero in bins 70-100 regardless of used η-gap. On the other hand, (1-2-1) layout leads to increasing trend with negative values of cumulant in low-multiplicity events. The larger η-gap does not provide better suppression of non-flow background in all bins except the bin 10-20, where the statistical fluctuations are strong. The compatibility with zero is achieved already in bins 50-100 for both η-gaps. Since PYTHIA is purely non-flow model, negative values of cumulant cannot be associated with collectivity in this case. This phenomenon is probably related to wide η-acceptance of ATLAS, which leads to the inclusion of long-range non-flow correlations (e.g. 3-jets). This is consistent with the previous observation of a larger effect of the η-gap size in low-multiplicity events.

5.3.3 More detailed study with the injected flow

The injected flow allows us to study the differences in the results obtained with different acceptances of detectors or specific aspects of the multiparticle cumulant method and the subevent method in more detail. The results in the previous sections 5.3.1 and 5.3.2 have proven that the subevent method lowers the magnitude of the flow signal. Since the decrease of the signal leads to the compatibility with zero,

especially in the measurements of the 4-particle cumulant in Fig. 5.3, it is meaningful to expect that the decrease is due to suppression of non-flow. The concept of injected flow allows us to study which method successfully reconstructs the injected signal and therefore to better understand the effect of the subevent method under different conditions.

Two different magnitudes of the injected flow were used in our measurements. The first used magnitude $v_{2_{in}} = 0.04$ was selected as the approximate expected value of the elliptic flow in pp collisions according to the experimental results of flow measurements done at ALICE and CMS [22, 18]. To see how different the results would be with a much larger magnitude of injected flow, we used another magnitude of the injected signal $v_{2_{in}} = 0.1$. The injected flow signal is illustrated by the dashed red line in all following measurements. Reconstruction of the injected flow is successful if the measured values are compatible with this plotted red line.

The first part of the following section is devoted to the general measurements of 2-particle and 4-particle cumulants and the ability of the subevent method to successfully suppress the non-flow background and thereby reconstruct the injected signal. The second part is focused on the comparison of two layouts of the 3-subevent method. Both parts include results obtained using both ALICE and ATLAS acceptances.

2-particle cumulant

In the left panel of Fig. 5.5 the dependence of two-particle cumulant $c_2\{2\}$ on multiplicity in pp collisions at the centre-of-mass energy $\sqrt{s} = 13\,\text{TeV}$ using ALICE acceptance can be observed. The 2-subevent method was used and the magnitude of the injected flow is $v_{2_{in}} = 0.04$. Regardless of the size of the η-gap, significant multiplicity dependence can be observed due to dominant non-flow contributions in the PYTHIA model. The overall trend is decreasing except bins 70-100, where the statistical fluctuations are large. As we can see, even with the largest η-gap our results are not reaching the injected signal, suggesting possible remaining non-flow contamination. It indicates that the 2-particle cumulant $c_2\{2\}$ is not a suitable observable for measuring a flow signal of this magnitude.

The right panel of Fig. 5.5 is devoted to same measurement obtained with ATLAS acceptance. Similar decreasing trend of the cumulant is observed, but the injected signal is not reconstructed even in this case due to remaining non-flow background.

The additional results obtained with the injected flow of the magnitude $v_{2_{in}} = 0.1$ can be found in Fig. A.3 in Appendix. It turns out that the larger magnitude of the injected flow does not lead to easier reconstruction of injected signal, because the non-flow background cannot be sufficiently suppressed.

4-particle cumulant

The measurement of the 4-particle cumulant $c_2\{4\}$ dependence on multiplicity in pp collisions at the centre-of-mass energy $\sqrt{s} = 13\,\text{TeV}$ using ALICE acceptances
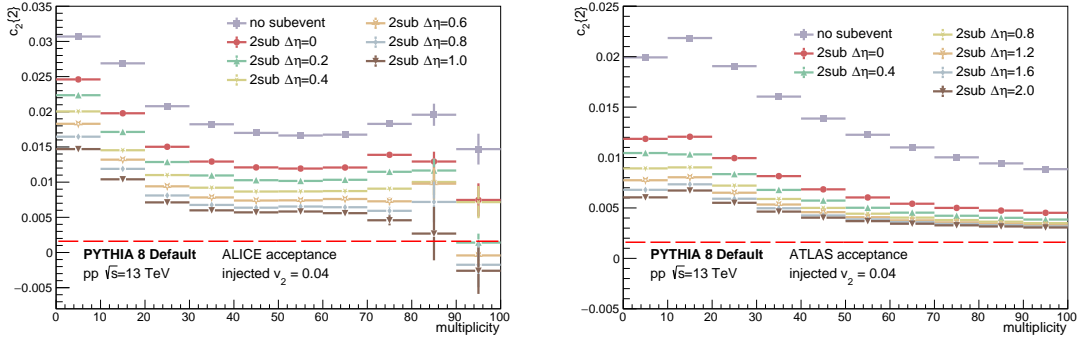
Figure 5.5: The two-particle cumulant $c_2\{2\}$ dependence on multiplicity with injected flow signal $v_{2_{in}} = 0.04$ using ALICE (left) and ATLAS (right) acceptances with the 2-subevent method with η-gaps of different sizes.

is in Fig. 5.6 (left). In order to suppress non-flow background, the 2-subevent or 3-subevent method (1-1-1 layout) with $\Delta\eta = 0$ are used. The magnitude of the injected signal is $v_{2_{in}} = 0.04$. The trend is decreasing reaching the compatibility with the injected signal in bin 50-60 with the 3-subevent method similarly to the ATLAS measurement in section 5.3.1 (Fig. 5.3). Bins 0-10 and 80-100 are empty due to large statistical fluctuations associated with either a small number of particles in the correlations or a small number of collisions overall. The values in bins 60-80 are dominated by statistical fluctuations caused by small number of events. As can be seen, only with the 3-subevent method it is possible to reconstruct the injected flow, but only in one bin at high-multiplicity events. Other methods failed to reconstruct the signal over the entire multiplicity range.

In the right panel of Fig. 5.6 we can see same measurement with the injected signal $v_{2_{in}} = 0.1$. Bins 0-10 and 60-100 are empty or containing values dominated by statistical fluctuations due to previously mentioned reasons. In this case the compatibility with the injected flow is achieved in bins 30-60 using the 3-subevent method. In addition, both the measurement without the subevent method and with the 2-subevent method successfully reconstruct the injected signal in these bins. It means that the increased magnitude of the injected flow signal leads to an improvement of the reconstruction and therefore we can assume that the reconstruction ability is dependent on the balance between the magnitude of the non-flow signal naturally present in PYTHIA and the magnitude of the artificially added flow signal. The more dominant the injected signal is, the better it is reconstructed. In the left panel of Fig. 5.6 the non-flow background is dominant, but in the second measurement (right panel) the non-flow background and the injected signal are more balanced.

Similarly we can investigate same measurement of the 4-particle cumulant $c_2\{4\}$ in pp collisions at the centre-of-mass energy $\sqrt{s} = 13\,\mathrm{TeV}$ using ATLAS acceptance. Firstly, let us observe results with the injected signal $v_{2_{in}} = 0.04$ in the left panel of Fig. 5.7. The first bin is empty due to small number of particles in correlations. The trend is decreasing for all configurations with or without the subevent method. Due to overall lower non-flow contamination of ATLAS results thanks to wider η-acceptance of the detector the compatibility with the injected flow is reached
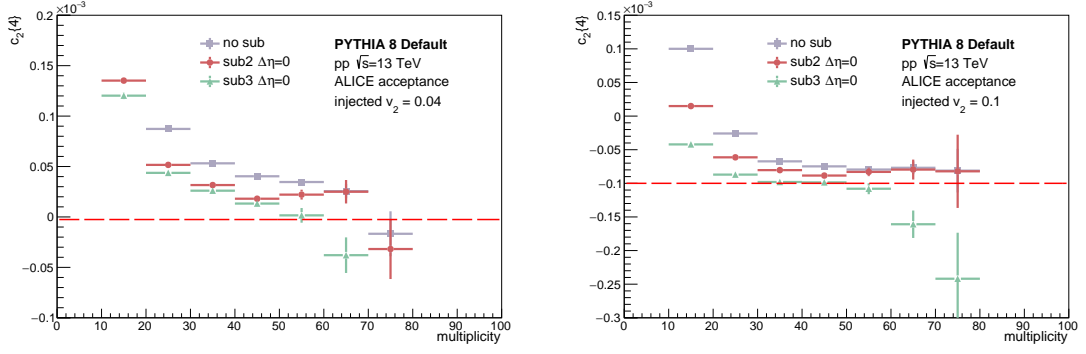
Figure 5.6: The 4-particle cumulant $c_2\{4\}$ dependence on multiplicity with injected flow signal $v_{2_{in}} = 0.04$ (left) or $v_{2_{in}} = 0.1$ (right) using ALICE acceptance with the 2 or 3-subevent method with $\Delta\eta = 0$.
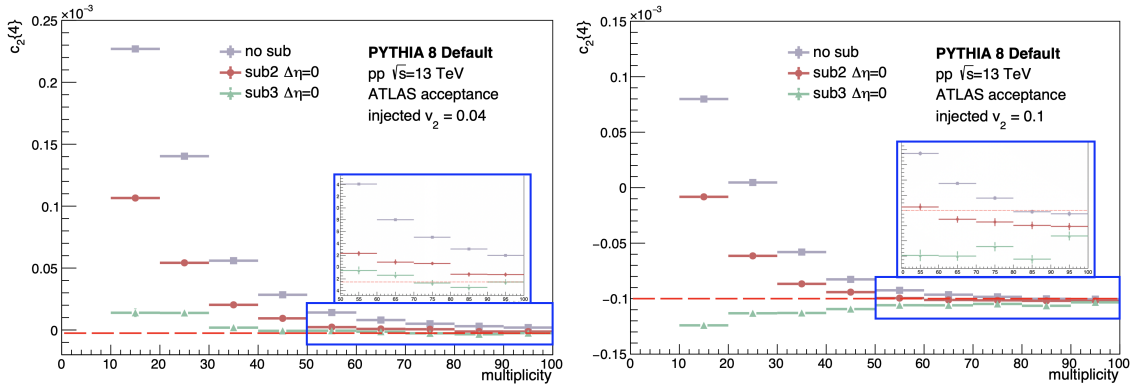

Figure 5.7: The 4-particle cumulant $c_2\{4\}$ dependency on multiplicity with injected flow signal $v_{2_{in}} = 0.04$ (left) or $v_{2_{in}} = 0.1$ (right) using ATLAS acceptance with the 2 or 3-subevent method with $\Delta\eta = 0$.

in more bins than in ALICE case. Specifically, the 3-subvent method is precisely compatible in bins 70-80 and 90-100, but also the 2-subevent method is almost reaching compatibility with the injected flow in high-multiplicity events. On the other hand, investigation of results with the injected flow $v_{2_{in}} = 0.1$ in the right panel of Fig. 5.7 shows that a larger injected signal leads to a reversal of the trend and an overestimation of the injected flow in the 3-subevent method. This suggests that in case of large acceptance of ATLAS, the method may not be suitable anymore for measurements of flow signal of the order of $v_{2_{in}} = 0.1$ or higher.

In summary, we have observed that the 3-subevent method provides efficient non-flow suppression, which leads, especially in ATLAS case, to a successful reconstruction of the injected flow signal of the magnitude $v_{2_{in}} = 0.04$. The larger magnitude of the injected signal $v_{2_{in}} = 0.1$ may lead to biased results. Even so, this method remains suitable, because the maximum expected flow in pp collisions is of the order of $v_2 = 0.06$ [22, 18].
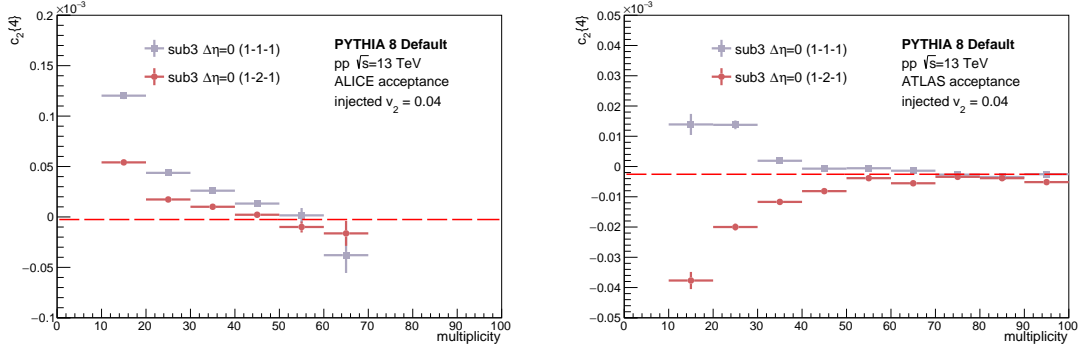
Figure 5.8: The 4-particle cumulant $c_2\{4\}$ dependency on multiplicity using ALICE (left) and ATLAS acceptances with two different layouts of the 3-subevent method with $\Delta\eta = 0$ and injected flow signal $v_{2_{in}} = 0.04$.

Different layouts of the 3-subevent method

The 4-particle cumulant $c_2\{4\}$ dependency on multiplicity in *pp* collisions at the centre-of-mass energy $\sqrt{s} = 13$ TeV using ALICE acceptance is in Fig. 5.8 (left). Two different layouts of the 3-subevent method described in the previous sections with $\Delta\eta = 0$ are applied and the magnitude of the injected flow signal is $v_{2_{in}} = 0.04$. Bins 0-10 and 70-100 are empty due to already mentioned reasons. The trend is decreasing for both layouts reaching compatibility with the injected signal in bins 40-70 in (1-2-1) configuration and only in bin 50-60 in (1-1-1) layout. It seems that (1-2-1) configuration provides more efficient non-flow suppression and therefore better reconstruction of the injected flow signal, which would be compatible with the conclusion in section 5.3.2. But if we look at Fig. A.4 (left) in Appendix (same measurement with larger added signal $v_{2_{in}} = 0.1$) we can see that this layout tends to overestimate injected flow in case of larger magnitude of the injected flow.

Similar measurement using ATLAS acceptance is plotted in the right panel of Fig. 5.8. The first bin is again empty due to the small number of particles for computation of the 4-particle correlation. The layout denoted here as (1-1-1) leads to a decreasing trend, and the compatibility of the injected signal and our results is achieved in bins 60-100. On the other hand, the result obtained with (1-2-1) configurations follows an decreasing trend, and the compatibility of the injected signal and our results is achieved in bins 70-90. The reversal of the trend emerging in this measurement is similar to ATLAS results in section 5.3.2 (Fig. 5.4) and is probably connected with the wider η-acceptance of ATLAS detector.

In result, we have seen that the reconstruction ability of the 3-subevent method depends on chosen layout. The configuration (1-2-1) leads to better result with the η-acceptance of ALICE detector using adequate magnitude of the injected flow signal $v_{2_{in}} = 0.04$, but with the η-acceptance of ATLAS detector an unexpected reversal of the trend happens.

Chapter 6

Jets in the multiparticle cumulant method

The second objective of this diploma thesis is a study of the effect of jets on the multiparticle cumulant method in collisions of small systems. Special attention is paid to the suppression of non-flow background using the subevent method. The same dataset of 2 billion *pp* collisions generated in PYTHIA as in the previous chapter was used in our analysis, and additionally FastJet library for jet finding was used.

Since the workflow is in this case very similar to the previous case, the chapter begins only with a brief introduction containing PYTHIA and FastJet settings and new steps of the analysis workflow. The second part is devoted to the results of the study.

6.1   Settings and analysis workflow

6.1.1   FastJet settings

As we have already mentioned, a C++ library called FastJet is used for jet finding in our case. FastJet implementation of k_t algorithm with $R = 0.3$ is used for background estimation and implementation of anti-k_t algorithm with $R = 0.4$ is used for reconstruction of true jets. Only jets that satisfy the condition $p_{T_{jet}} > 5\,\mathrm{GeV}$ are considered and a fiducial cut according to relation $\eta_{jet} > \eta_{det} - R$ (η_{det} is an acceptance of a detector) is applied.

6.1.2   Differences in workflow

The analysis workflow sketched in section 5.1.3 is not extended in this case. The only change is done in the macro that generates events using PYTHIA. Along with the already mentioned properties stored in particular TTrees, 4-vectors of all particles

are stored in *PseudoJet* objects and the particles are indexed for later identification of which particle is part of a specific jet. The background is then estimated, cuts are applied and jets are reconstructed. Finally, the properties of the jets (e.g. p_T of the jet or the number of particles in the jet) are stored in another TTree and the particles that are constituents of the jets are labelled.

6.2   Results

The following section contains measurements of 2-particle and 4-particle cumulants using both ALICE and ATLAS acceptances. Our main goal is to study how the non-flow correlations from jets affect the multiplicity dependencies of various cumulants and to investigate which configuration of the subevent method is most effective in suppressing these non-flow contributions. Firstly, cumulants computed using only particles that are constituents of jets are shown (marked as *ONLY JETS*) in order to study in which events these contributions are most dominant and how effectively they are suppressed using the subevent method. Afterwards, cumulants computed using only particles that are not constituents of jets are shown (marked as *WITH-OUT JETS*) to see how strong the non-flow background is after jet correlations are subtracted and whether it can be suppressed using the subevent method.

6.2.1   2-particle cumulant

The measurement of the 2-particle cumulant $c_2\{2\}$ dependency on multiplicity in pp collisions at the centre-of-mass energy $\sqrt{s} = 13\,\text{TeV}$ using ALICE acceptance is in Fig. 6.1. The left part is devoted to results obtained using only particles that are constituents of jets and the right part are cumulants obtained using particles that are not jet constituents. The 2-subevent method with different η-gaps is used for non-flow suppression in both cases.

As we can see in the left panel of Fig. 6.1, the trend of cumulant $c_2\{2\}$ computed from jet particles is decreasing. The 2-subevent method provides efficient suppression of jet non-flow contributions. The compatibility of the cumulant with zero is achieved in high-multiplicity events with large η-gaps indicating near-perfect subtraction of jet related non-flow. The effect of the 2-subevent method with $\Delta\eta = 0, 0.2, 0.4$ in low-multiplicity events is negligible. On the other hand, the effect of larger η-gaps in low-multiplicity events is significant and the best suppression is achieved with the largest η-gap. In other bins, except the bin 90-100, where the trend is violated due to statistical fluctuations, there is apparent effect of the 2-subevent method with small η-gaps and unlike the low-multiplicity events the suppression effect is saturated for $\Delta\eta = 0.6, 0.8, 1.0$. Since jets in low-multiplicity events are more likely to be composed of fewer particles than in high-multiplicity events, the suppression provided by the subevent method in low-multiplicity events is more sensitive to the η-distribution of particles in particular jet. Consequently, different η-gaps sizes have different impacts on $c_2\{2\}$ in different multiplicity bins.
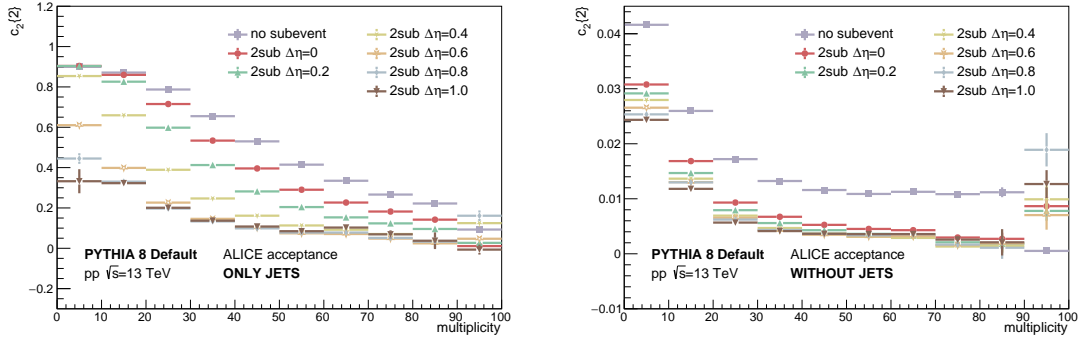
Figure 6.1: Multiplicity dependency of the two-particle cumulant $c_2\{2\}$ for ALICE acceptance using the 2-subevent method with different η-gaps computed from particles that are constituents of jets (left) and particles that are not (right).

The right panel of Fig. 6.1 is devoted to the measurement of $c_2\{2\}$ computed from particles that are not constituents of jets. The overall trend is very similar to other ALICE measurements of $c_2\{2\}$ in previous sections. The biggest difference is the effect of the 2-subevent method. As we can observe, a simple division of the η-acceptance with $\Delta\eta = 0$ provides the largest non-flow subtraction and further enlargement of the η-gap leads to only moderate additional suppression. It indicates that after the subtraction of jet related non-flow, the remaining non-flow origins mostly from decays of heavy particles. The products of these decays are collimated, so the basic layout of the 2-subevent method with $\Delta\eta = 0$ already provides a strong suppression, but the enlargement of the η-gap has only little effect. On the other hand, the non-flow jet related correlations are progressively more and more suppressed as the η-gap is getting bigger as we have already seen in the left panel of Fig. 6.1. The compatibility with zero in the measurement in the right panel of Fig. 6.1 is reached in high-multiplicity events, which indicates that subtraction of jet related non-flow by jet reconstruction and application of the 2-subevent method for additional suppression could provide almost complete removal of non-flow background even in the measurement of two-particle cumulant.

The previous measurements can be compared to results obtained with ATLAS acceptance in Fig. 6.2. The overall trend is decreasing in the first bins and rather constant for high-multiplicity events. In this case, a division of the η-acceptance with $\Delta\eta = 0$ provides the largest suppression of jet related non-flow background regardless of multiplicity, as we can see in the left panel. The enlargement of η-gap from $\Delta\eta = 0$ to 0.4 results in only a small increase in suppression.

In the right panel of Fig. 6.2, we can observe the measurement of $c_2\{2\}$ computed from particles that are not constituents of jets. Similarly to the ALICE case, the measurement has similar trend as the previous measurements of $c_2\{2\}$ for ATLAS acceptance. The suppression effect of the 2-subevent method with $\Delta\eta = 0$ remains the largest, but the enlargement of the η-gap is not negligible unlike the ALICE case. The compatibility with zero is achieved in an even larger number of high-multiplicity bins than in the ALICE measurement, suggesting that this approach can lead to the complete removal of non-flow in the $c_2\{2\}$ measurements.
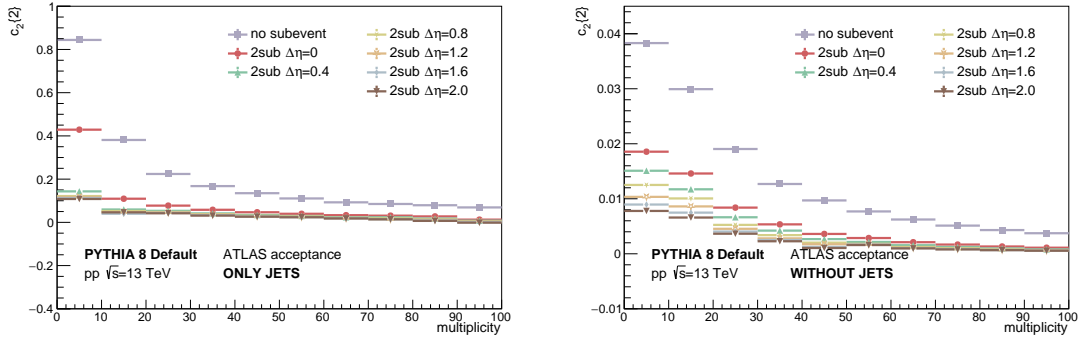
Figure 6.2: Multiplicity dependency of the two-particle cumulant $c_2\{2\}$ for ATLAS acceptance using the 2-subevent method with different η-gaps computed from particles that are constituents of jets (left) and particles that are not (right).

6.2.2 4-particle cumulant

In Fig. 6.3 we can observe the measurement of four-particle cumulant $c_2\{4\}$ in pp collisions at the centre-of-mass energy $\sqrt{s} = 13\,\mathrm{TeV}$ using ALICE acceptance. The effect of 2 and 3-subevent method with $\Delta\eta = 0$ is investigated.

Firstly, let us focus on the 4-cumulant computed from jet particles in the left panel of Fig. 6.3. As we can see, the value of the 4-particle cumulant $c_2\{4\}$ is negative. The negative contributions to the cumulant probably origin from long-range non-flow correlations between particles in di-jets. By correlating four particles instead of two, the jet related background is completely suppressed in high-multiplicity events, as $c_2\{4\}$ is found to be compatible with zero. The 2-subevent method provides significant non-flow suppression in bins 30-60. Since the 3-subevent method effectively suppresses di-jets, a significant additional non-flow subtraction is achieved after its application, especially in low-multiplicity events. Even with the 3-subevent method, negative values of $c_2\{4\}$ are obtained. It could be related to correlations from 3-jets that are not suppressed even by the 3-subevent method. At the same time, division of the limited ALICE acceptance into three small subevents may have reintroduced some of the short-range non-flow correlations that were already suppressed in the 2-subevent method. But these correlations would result in a positive signal, since the contribution of short-range correlations to the 4-particle cumulant is positive.

The right panel of Fig. 6.3 is devoted to the measurement of $c_2\{4\}$ computed from particles that are not constituents of jets. Bin 0-10 is empty due to a small number of particles in these collisions. Bins 70-100 are dominated by statistical fluctuations or empty due to statistical fluctuations caused by small number of such events. The overall trend is decreasing and the compatibility with zero is reached in events with intermediate multiplicity. As we can observe, the 4-particle cumulant computed without the subevent method never satisfy compatibility with zero except bin 70-80, where statistical fluctuations are very large. $c_2\{4\}$ computed with the subevent method is compatible with zero at intermediate multiplicity. In summary, to sufficiently suppress non-flow in these measurements, we should remove jet related correlations and additionally use the subevent method. This statement is illustrated
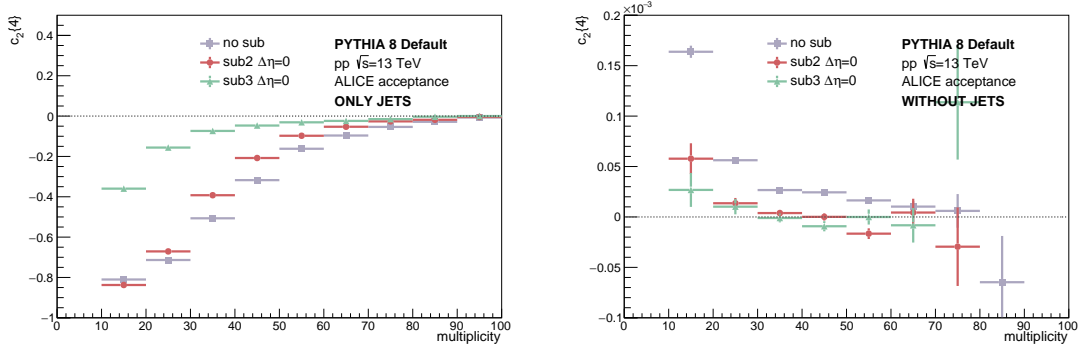
Figure 6.3: Multiplicity dependency of the four-particle cumulant $c_2\{4\}$ for ALICE acceptance using the 2 and 3-subevent method with $\Delta\eta = 0$ computed from particles that are constituents of jets (left) and particles that are not (right).

in Fig. 6.4, where we can observe a comparison of the 4-particle cumulant $c_2\{4\}$ computed from all particles and the 4-particle cumulant computed from those particles that are constituents of jets. The combination of the removal of jet particles with the 3-subevent method results in the compatibility with zero in bins 30-40 and 50-70 in this measurement.
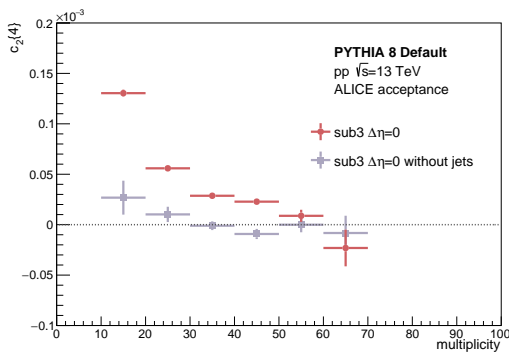

Figure 6.4: Multiplicity dependence of the 4-particle cumulant $c_2\{4\}$ for ALICE acceptance using the 3-subevent method with $\Delta\eta = 0$ computed from all particles and those particles that are constituents of jets.

The measurement of $c_2\{4\}$ using ATLAS acceptance is in Fig. 6.5. The trend is similar to the ALICE case, but the compatibility with zero without the subevent method is reached in even more bins (60-100). If the 2-subevent method is used, the compatibility is achieved additionally in bin 40-60. On the other hand, low-multiplicity events remain contaminated by jet related non-flow regardless of the subevent method. The conclusion is that jet related non-flow correlations in the $c_2\{4\}$ ATLAS measurements can be almost perfectly eliminated in collisions with intermediate and high multiplicity even without the subevent method.

As we can see in the the ATLAS measurement of $c_2\{4\}$ computed from particles that are not components of jets in the right panel of Fig. 6.5, the complete removal of non-flow background is achieved in bins 40-100 even without the subevent method.
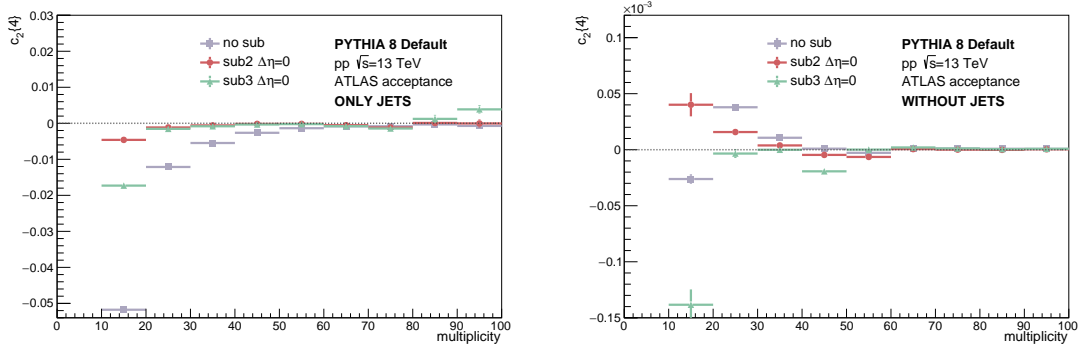
Figure 6.5: Multiplicity dependency of the four-particle cumulant $c_2\{4\}$ for ATLAS acceptance using the 2 and 3-subevent method with $\Delta\eta = 0$ computed from particles that are constituents of jets (left) and particles that are not (right).

The 2 and 3-subevent methods tend to overestimate the cumulant in bin 40-50. In low-multiplicity events, the cumulant obtained without the subevent method is decreasing significantly to negative values. The 2-subevent method reverses the trend of the measurement to positive values, but the 3-subevent method provides significantly negative values in low-multiplicity events. Particles from jets should be extracted in this measurement and the acceptance of ATLAS is wider than the ALICE acceptance. The origin of the negative $c_2\{4\}$ obtained using the 3-subevent method should then be different than in the ALICE measurement in the left panel of Fig. 6.3.

Conclusion

The CMS measurement of the two-particle correlation in high-multiplicity pp collisions in 2010 started a new era of collectivity investigation of small systems. Small collision systems, dominated by short-range non-global correlations called non-flow, indicated similar collective behaviour to heavy-ion collisions. To observe this collectivity, non-flow background must be strongly suppressed. The subevent method dividing the η-acceptance of the detector into several parts referred to as subevents and correlating only particles from different subevents, proved to be a very effective way to suppress non-flow background according to previous measurements. We have also seen that different acceptances of the detectors have a significant impact on flow measurements.

In order to study non-flow contamination and the suppression effect of the subevent method, we have implemented our own code for flow computation using the multi-particle cumulant method in the Generic Framework. It allowed us to modify the subevent method to investigate the suppression effect of different configurations of the method on results obtained using different acceptances of detectors.

The dataset of 2 billion pp collisions for our study was generated in a purely non-flow PYTHIA model. In previous studies, it was shown that $v_n\{2\}$ predicted by PYTHIA model is not compatible with experimental results and $v_n\{4\}$ cannot be compared to experimental results, since PYTHIA model does not predict the negative value of the 4-particle cumulant even with the subevent method [22]. Despite the fact that the results obtained using PYTHIA model are not directly comparable to experimental results, they are perfectly suitable for studies of non-flow suppression.

Firstly, we have compared the measurements of cumulants using ALICE and ATLAS acceptances. In both cases, the subevent method provides significant suppression of non-flow, increasing with the larger size of the η-gap between subevents. The ALICE measument of the $c_2\{2\}$ is dominated by short-range correlations due to the lower η-separation between particles resulting in stronger non-flow background than in the ATLAS measurements. The measurements of the two-particle cumulant remain contaminated by non-flow even with large η-gaps. The measurements of the four-particle cumulant $c_2\{4\}$ show further suppression of non-flow. The four-particle cumulant suppresses two-particle non-flow correlations by definition and therefore the signal is decreasing. The ALICE measurement remains contaminated by non-flow even with the use of the 3-subevent method, because the values of $c_2\{4\}$ remain positive in all multiplicity bins. On the other hand, the compatibility of the cumulant with zero is reached in high-multiplicity events in the ATLAS measurement.

Secondly, the two different layouts of the 3-subevent method were studied. We have observed stronger non-flow background using (1-1-1) configuration with all subevents of the same size in the ALICE measurement of the $c_2\{4\}$. Using the other layout (1-2-1) with the middle subevent twice as large as others may lead to a better separation of a single jet cone in the middle subevent and a larger η-separation between edge particles from outer and middle subevents, which results in a weaker non-flow background. Therefore, we can conclude that the (1-2-1) configuration is more suitable for the ALICE acceptance. On the other hand, in the ATLAS measurement, two different layouts lead to opposite trends of the $c_2\{4\}$ in low-multiplicity events. The (1-2-1) configuration gives a negative values of cumulant, which is probably linked to the inclusion of long-range non-flow correlations from 3-jets. Unlike the ALICE case, the (1-1-1) configuration turned out to be more more suitable for the ATLAS acceptance.

The previous studies have shown that the use of the subevent method in the multi-particle cumulants suppresses non-flow significantly and that different acceptances of detectors lead to different results. To find out if the method is suitable for detection of a flow signal hidden behind strong non-flow background, we need to simulate a more realistic situation close to the experimental measurements. For these purposes, we introduce the concept of the injected flow. It allows us to study, which method leads to the best reconstruction of artificially introduced flow signal and therefore suppress the non-flow background in a most effective way.

We have seen that the two-particle cumulant $c_2\{2\}$ never reaches compatibility with the injected signal regardless of the size of the used η-gap and the magnitude of the flow signal. The compatibility with the injected signal is reached in the measurement of the 4-particle cumulant $c_2\{4\}$. In the ALICE case, the injected signal of the magnitude $v_{2_{in}} = 0.04$ cannot be successfully reconstructed, because the measurement is not compatible with the injected flow except for one bin. On the other hand, injected flow of the larger magnitude $v_{2_{in}} = 0.1$ can be reconstructed using the 3-subevent method in intermediate and high-multiplicity bins. It brings us to the conclusion that the successful reconstruction of the injected signal depends on the balance between the magnitude of the non-flow signal and the magnitude of the injected flow. The results obtained with the 3-subevent method using the ATLAS acceptance are precisely compatible with the injected signal $v_{2_{in}} = 0.04$ in high-multiplicity events thanks to the lower non-flow contamination due to the wider η-acceptance. Although it was observed that the injected flow of a larger magnitude $v_{2_{in}} = 0.1$ leads to biased results, the method remains suitable, because the flow in pp collisions is expected not to exceed $v_2 = 0.06$ [22, 18]. The different layouts of the 3-subevent method can be studied also with the concept of the injected flow. Our measurements revealed that the (1-2-1) configuration leads to better results with the ALICE η-acceptance using adequate magnitude of the injected signal ($v_{2_{in}} = 0.04$), but in the case of ATLAS detector a significant reversal of the trend, probably linked to the wide η-acceptance of ATLAS, happens.

One of the largest contributors to non-flow contamination in small collision systems is correlations from particles that are constituents of jets. In order to study the suppression effect of the subevent method on these specific correlations, we have

used FastJet library using anti-k_t algorithm with $R = 0.4$ for jet reconstruction.

The measurement of the two-particle cumulant $c_2\{2\}$ using the ALICE acceptance showed that, after the extraction of jet particles, the remaining non-flow can be mostly suppressed by a simple division of the η-acceptance with $\Delta\eta = 0$, which indicates that these remaining non-flow correlations origins from collimated decay products. Since the compatibility of the $c_2\{2\}$ with zero is achieved in high-multiplicity events, we can conclude that subtraction of jet particles together with the 2-subevent method may lead to an almost complete removal of non-flow background even in this measurement, which is heavily contaminated as we have seen. The measurement of the $c_2\{2\}$ obtained with the 2-subevent method and using the ATLAS acceptance leads to the similar conclusion, since the compatibility with zero is reached in a larger number of high-multiplicity bins.

In the ALICE case, we have seen that the removal of jet particles together with the 3-subevent method leads to the compatibility of the 4-particle cumulant with zero in intermediate and high-multiplicity bins. The same observation can be made in the ATLAS measurement of the 4-particle cumulant. The difference is that in the ATLAS case we were able to achieve $c_2\{4\} \sim 0$ (i.e. completely suppress non-flow) even without the removal of jet particles, but the ALICE measurements remained contaminated. Only the combination of removing jet related non-flow with the 3-subevent method resulted in the 4-particle cumulant compatible with zero in intermediate and high-multiplicity events in the ALICE measurement. This combination is useful also in the ATLAS measurement, because it allows us to measure contamination-free non-flow at lower multiplicities. Finally, we can conclude that the subtraction of jet particles together with the 3-subevent method used in computation of the 4-particle cumulant $c_2\{4\}$ can lead to a complete suppression of non-flow regardless of the acceptance of the detector.

The aim of this thesis was to investigate how non-flow contamination affects experimental results of ALICE and ATLAS experiments. It turned out that the ALICE results could be contaminated by larger residual non-flow background than the ATLAS results. The (1-2-1) layout of the 3-subevent method currently used at ALICE experiment may not be sufficient to suppress non-flow, especially in low-multiplicity events. It may be linked to the differences in the measurements of $SC_{3,2}$ at both experiments. According to our observations, the most suitable way to measure flow in small systems is to remove particles that are constituents of jets and use the 4-particle cumulant $c_2\{4\}$ computed using the 3-subevent method. A very large number of collisions need to be recorded to achieve sufficient statistics, but it should be possible in Run 3 at the LHC.

Bibliography

[1] Y. Aoki, Z. Fodor, S. D. Katz, and K. K. Szabo. The QCD transition temperature: Results with physical masses in the continuum limit. *Phys. Lett. B*, 643:46–54, 2006.

[2] Betty Abelev et al. Pion, Kaon, and Proton Production in Central Pb–Pb Collisions at $\sqrt{s_{NN}} = 2.76$ TeV. *Phys. Rev. Lett.*, 109:252301, 2012.

[3] R. Stock. Relativistic Nucleus-Nucleus Collisions and the QCD Matter Phase Diagram. 7 2008.

[4] Michael Kliemant, Raghunath Sahoo, Tim Schuster, and Reinhard Stock. *Global Properties of Nucleus–Nucleus Collisions*, pages 23–103. Springer Berlin Heidelberg, Berlin, Heidelberg, 2010.

[5] Fabian Rennecke. Review of Critical Point Searches and Beam-Energy Studies. *MDPI Proc.*, 10(1):8, 2019.

[6] Lokesh Kumar. Review of Recent Results from the RHIC Beam Energy Scan. *Mod. Phys. Lett. A*, 28:1330033, 2013.

[7] Roman Kogler et al. Jet Substructure at the Large Hadron Collider: Experimental Review. *Rev. Mod. Phys.*, 91(4):045003, 2019.

[8] Amanda M. Cooper-Sarkar, R. C. E. Devenish, and A. De Roeck. Structure functions of the nucleon and their interpretation. *Int. J. Mod. Phys. A*, 13:3385–3586, 1998.

[9] James L. Nagle and William A. Zajc. Small System Collectivity in Relativistic Hadronic and Nuclear Collisions. *Ann. Rev. Nucl. Part. Sci.*, 68:211–235, 2018.

[10] Carlos A. Salgado and Johannes P. Wessels. Proton–Lead Collisions at the CERN LHC. *Ann. Rev. Nucl. Part. Sci.*, 66:449–473, 2016.

[11] Maria Vasileiou. Transverse momentum spectra and nuclear modification factors of identified charged hadrons in p-pb and pb-pb collisions at s nn = 5.02 tev with alice. *EPJ Web of Conferences*, 182:02126, 01 2018.

[12] Vardan Khachatryan et al. Observation of Long-Range Near-Side Angular Correlations in Proton-Proton Collisions at the LHC. *JHEP*, 09:091, 2010.

[13] Kevin Dusling, Wei Li, and Björn Schenke. Novel collective phenomena in high-energy proton–proton and proton–nucleus collisions. *Int. J. Mod. Phys. E*, 25(01):1630002, 2016.

[14] Jaroslav Adam et al. Anisotropic flow of charged particles in Pb-Pb collisions at $\sqrt{s_{\mathrm{NN}}}$ = 5.02 TeV. *Phys. Rev. Lett.*, 116(13):132302, 2016.

[15] Morad Aaboud et al. Measurement of multi-particle azimuthal correlations in pp, p+Pb and low-multiplicity Pb+Pb collisions with the ATLAS detector. *Eur. Phys. J. C*, 77(6):428, 2017.

[16] Jaroslav Adam et al. Correlated event-by-event fluctuations of flow harmonics in Pb-Pb collisions at $\sqrt{s_{\mathrm{NN}}}$ = 2.76 TeV. *Phys. Rev. Lett.*, 117:182301, 2016.

[17] Morad Aaboud et al. Correlated long-range mixed-harmonic fluctuations measured in pp, p+pb and low-multiplicity pb+pb collisions with the atlas detector. *Physics Letters B*, 789:444–471, 2019.

[18] Vardan Khachatryan et al. Evidence for collectivity in pp collisions at the LHC. *Phys. Lett. B*, 765:193–220, 2017.

[19] Betty Abelev et al. Long-range angular correlations on the near and away side in p-Pb collisions at $\sqrt{s_{NN}}$ = 5.02 TeV. *Phys. Lett. B*, 719:29–41, 2013.

[20] Georges Aad et al. Observation of Associated Near-Side and Away-Side Long-Range Correlations in $\sqrt{s_{NN}}$=5.02 TeV Proton-Lead Collisions with the ATLAS Detector. *Phys. Rev. Lett.*, 110(18):182302, 2013.

[21] Serguei Chatrchyan et al. Observation of Long-Range Near-Side Angular Correlations in Proton-Lead Collisions at the LHC. *Phys. Lett. B*, 718:795–814, 2013.

[22] Shreyasi Acharya et al. Investigations of Anisotropic Flow Using Multiparticle Azimuthal Correlations in pp, p-Pb, Xe-Xe, and Pb-Pb Collisions at the LHC. *Phys. Rev. Lett.*, 123(14):142301, 2019.

[23] C. Aidala et al. Creation of quark–gluon plasma droplets with three distinct geometries. *Nature Phys.*, 15(3):214–220, 2019.

[24] Shen Schenke and Tribedy. Small system scan within a combined color glass condensate and hydrodynamic model. *Quark Matter 2019*, 2019.

[25] Zuzana Moravcova. Observation of partonic flow in small collision systems with alice at the lhc.

[26] Morad Aaboud et al. Measurement of long-range multiparticle azimuthal correlations with the subevent cumulant method in pp and $p + Pb$ collisions with the ATLAS detector at the CERN Large Hadron Collider. *Phys. Rev. C*, 97(2):024904, 2018.

[27] Ante Bilandzic, Christian Holm Christensen, Kristjan Gulbrandsen, Alexander Hansen, and You Zhou. Generic framework for anisotropic flow analyses with multiparticle azimuthal correlations. *Phys. Rev. C*, 89(6):064904, 2014.

[28] Jiangyong Jia, Mingliang Zhou, and Adam Trzupek. Revealing long-range multiparticle collectivity in small collision systems via subevent cumulants. *Phys. Rev. C*, 96(3):034906, 2017.

[29] Torbjörn Sjöstrand, Stefan Ask, Jesper R. Christiansen, Richard Corke, Nishita Desai, Philip Ilten, Stephen Mrenna, Stefan Prestel, Christine O. Rasmussen, and Peter Z. Skands. An introduction to PYTHIA 8.2. *Comput. Phys. Commun.*, 191:159–177, 2015.

[30] Christian Bierlich, Gösta Gustafson, and Leif Lönnblad. Diffractive and non-diffractive wounded nucleons and final states in pA collisions. *JHEP*, 10:139, 2016.

[31] Matteo Cacciari, Gavin P. Salam, and Gregory Soyez. FastJet user manual. *The European Physical Journal C*, 72(3), mar 2012.

[32] Peter Skands, Stefano Carrazza, and Juan Rojo. Tuning PYTHIA 8.1: the Monash 2013 Tune. *Eur. Phys. J. C*, 74(8):3024, 2014.

[33] M. Masera, G. Ortona, M. G. Poghosyan, and F. Prino. Anisotropic transverse flow introduction in monte carlo generators for heavy ion collisions. *Phys. Rev. C*, 79:064909, Jun 2009.

Appendix A

Additional results

A.1 Comparison of ALICE and ATLAS acceptances

The measurement of the 2-particle cumulant $c_2\{2\}$ dependency on multiplicity for ALICE and ATLAS acceptances at the centre-of-mass energy $\sqrt{s} = 13\,\text{TeV}$ in pp collisions is in Fig. A.1. Different η-gaps in the 2-subevent method are used.

A.2 Study of different layouts of the 3-subevent method

In Fig. A.4 dependence of the 4-particle cumulant $c_2\{4\}$ on multiplicity for ALICE (left) and ATLAS (right) acceptances can be observed. Two different layouts of the 3-subevent method with $\Delta\eta = 0$ and 0.2 are used.
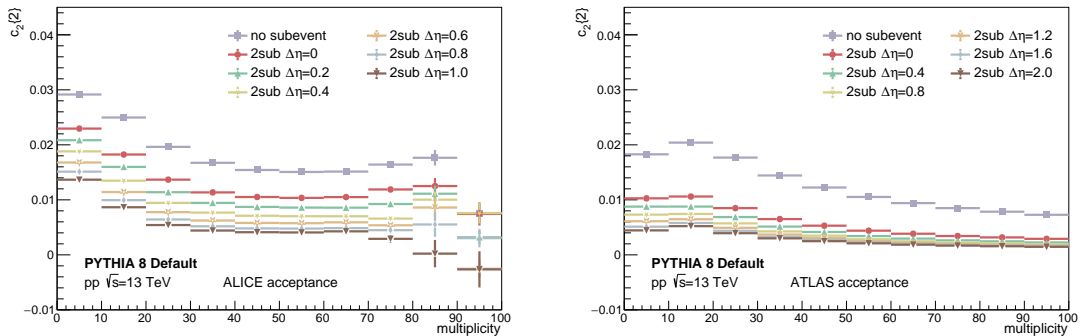

Figure A.1: The two-particle cumulant $c_2\{2\}$ dependency on multiplicity for ALICE (left) and ATLAS (right) acceptances using 2-subevent method with different η-gaps.
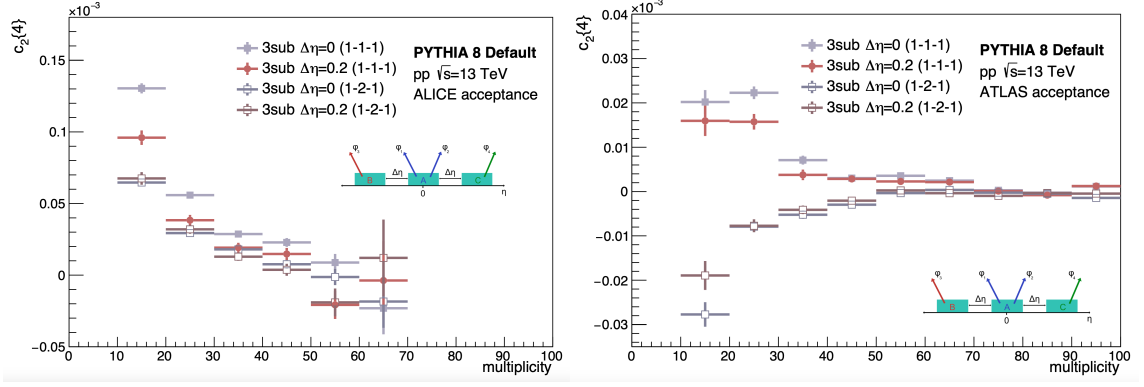
Figure A.2: The four-particle cumulant $c_2\{4\}$ dependence on multiplicity of ALICE (left) and ATLAS (right) acceptances using 3-subevent method with $\Delta\eta = 0, 0.2$ and two different configurations (1-1-1) and (1-2-1) described in the text.
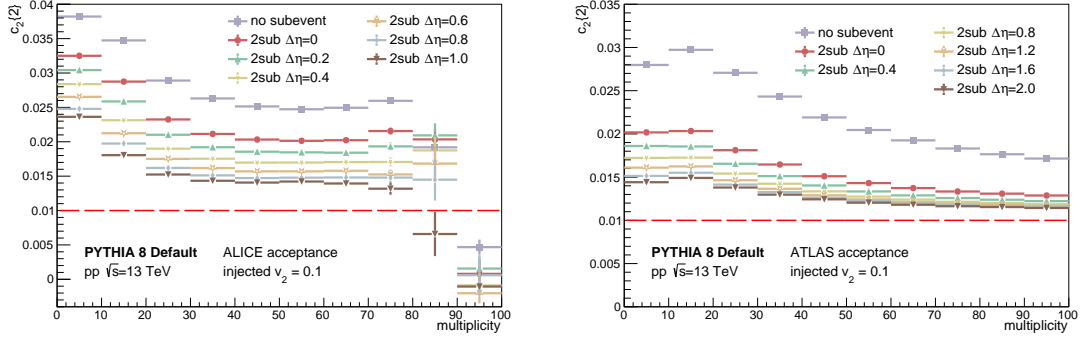

Figure A.3: The two-particle cumulant $c_2\{2\}$ dependence on multiplicity with injected flow signal $v_{2_{i}n} = 0.1$ using ALICE (left) and ATLAS (right) acceptances with the 2-subevent method with η-gaps of different sizes.

A.3 Study of multi-particle cumulant method with the injected flow

In Fig. A.3 dependence of the two-particle cumulant $c_2\{2\}$ on multiplicity for ALICE (left) and ATLAS (right) acceptances can be observed. The 2-subevent method is used and the magnitude of injected flow is $v_{2_{i}n} = 0.1$.

A.4 Study of different layouts of the 3-subevent method with the injected flow

In Fig. A.4 dependence of the 4-particle cumulant $c_2\{4\}$ on multiplicity for ALICE (left) and ATLAS (right) acceptances can be observed. Two different layouts of the 3-subevent method with $\Delta\eta = 0$ are used and the magnitude of the injected flow signal is $v_{2_{in}} = 0.1$.
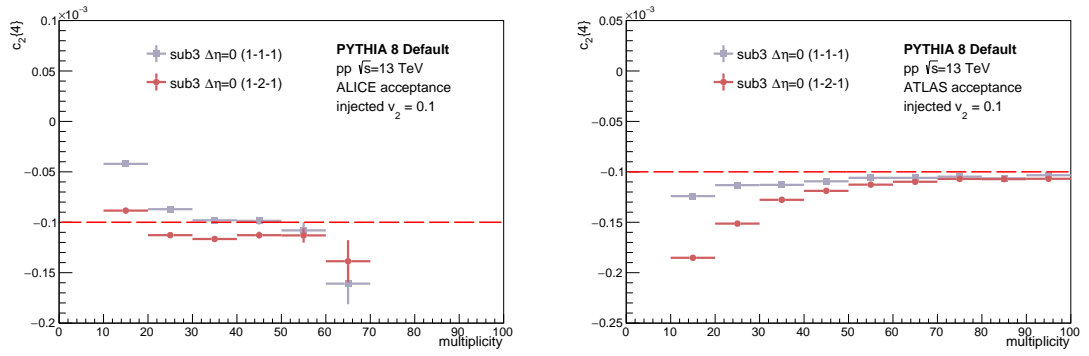
Figure A.4: The 4-particle cumulant $c_2\{4\}$ dependence on multiplicity using ALICE (left) and ATLAS acceptances with two different layouts of the 3-subevent method with $\Delta\eta = 0$ and injected flow signal $v_{2_{in}} = 0.1$.